

JOURNAL OF ICIVILTECH

INNOVATIONS IN CIVIL ENGINEERING AND TECHNOLOGY

YEAR: **2022** VOLUME: **4** ISSUE: **2**

EARTHQUAKE **ENGINEERING**

BUILDING MATERIALS **ENGINEERING**

STRUCTURAL **ENGINEERING**

CONSTRUCTION MANAGEMENT **ENGINEERING**

TRANSPORTATION **ENGINEERING**

GEOTECHNICAL **ENGINEERING**

e-ISSN: 2687-2129

HYDRAULIC AND WATER RESOURCES **ENGINEERING**

Journal of Innovations in Civil Engineering and Technology

(JICIVILTECH)

2022, Volume 4, Issue 2

The Journal Information

Publisher: Hüseyin AKBULUT

Editor-in-Chief: Hüseyin AKBULUT

Editors: Cahit GÜNER, Gökhan GÖRHAN, Gökhan KÜRKLÜ

Field Editor: Murat HİÇYILMAZ

Secretary of Publication: Ayfer ELMACI, Burak Enis KORKMAZ, Şule YARCI

Access: Open Access

Language of Publication: English and Turkish

Publication Frequency: Twice a year (in December and June)

Type of Publication: Peer-reviewed and periodical

e-ISSN: 2687-2129

Telephone: +90 272 2182 30 00 (2324)

E-mail: j.civiltech@gmail.com

Webpage: <https://dergipark.org.tr/tr/pub/jiciviltech>

Correspondence Address: Afyon Kocatepe University, Engineering Faculty, Civil Engineering Department, Ahmet Necdet Sezer Campus, 03200, Afyonkarahisar, TURKEY.

Advisory Board of the 2nd Issue

Reviewer List of the 2nd Issue

Ahmet Raif BOĞA, *Afyon Kocatepe University, Turkey*
Ahmet YILDIZ, *Afyon Kocatepe University, Turkey*
Alan WOODSIDE, *Brunel University, United Kingdom*
Bojan ZLENDER, *University of Maribor, Slovenia*
Dunja PERIC, *Kansas State University, United States*
Erol TUTUMLUER, *University Of Illinois At Urbana-Champaign, United States*
Hasan TOSUN, *Eskisehir Osmangazi University, Turkey*
Hashem R. AL-MASAEID, *Jordan University of Science and Technolgy, Jordan*
Hüseyin Yılmaz ARUNTAŞ, *Gazi University, Turkey*
Imad L. AL-QADI, *University Of Illinois At Urbana-Champaign, United States*
Iqbal KHAN, *King Saud University, Saudi Arabia*
Ivanka NETINGER, *University of Osijek, Croatia*
İlhami DEMİR, *Kırıkkale University, Turkey*
İsmail DEMİR, *Afyon Kocatepe University, Turkey*
João Pedro SILVA, *Polytechnic Institute of Leiria, Portugal*
Masayasu OHTSU, *Kyoto University, Japan*
Mehmet SALTAN, *Süleyman Demirel University, Turkey*
Meltem SAPLIOĞLU, *Suleyman Demirel University, Turkey*
Meor Othman HAMZAH, *University Sains Malaysia, Malaysia*
Mujib RAHMAN, *Brunel University, United Kingdom*
Murat KANKAL, *Uludağ University, Turkey*
Murat Vergi TACIROĞLU, *Mersin University, Turkey*
Paula FOLINO, *University of Buenos Aires, Argentina*
Roumiana ZAHARIEVA, *University of Architecture, Bulgaria*
Serdal TERZİ, *Süleyman Demirel University, Turkey*
Sri Atmaja P. ROSYIDI, *Muhammadiyah University of Yogyakarta, Indonesia*
Tamer BAYBURA, *Afyon Kocatepe University, Turkey*
Veli BAŞARAN, *Afyon Kocatepe University, Turkey*

Kanat Burak BOZDOĞAN, *Çanakkale Onsekiz Mart University, Turkey*
Kemal Muhammet ERTEN, *Isparta University of Applied Sciences, Turkey*
Mehmet CANBAZ, *Eskişehir Osmangazi University, Turkey*
Hümeyra BOLAKAR TOSUN, *Aksaray University, Turkey*
Meltem SAPLIOĞLU, *Suleyman Demirel University, Turkey*
Özlem ÇALIŞKAN, *Bilecik Şeyh Edebali University, Turkey*

Contents / İçindekiler

Articles / Makaleler	Sayfa
Muhammed Fatih YENTİMUR, Tuba KÜTÜK-SERT, Sezai KÜTÜK Bor ve Bor Atığının İnşaat Yıkıntı Atığı ile Normal Beton Üzerindeki Etkileri <i>Effects of Boron and Boron Waste with Recycling Aggregate on Normal Concrete</i>	47-60
Fethullah USLU, Mustafa Halûk SARAÇOĞLU, Uğur ALBAYRAK Buckling of Square and Circular Perforated Square Plates under Uniaxial Loading <i>Tek Eksenli Yükleme Altındaki Kare ve Dairesel Delikli Kare Plakların Burkulması</i>	61-75
Teh Sek Yee, Tan Shin Ru, Meor Othman Hamzah, Seyed Reza Omranian, Mohd Rosli Hainin Evaluation of the Combined Effects of Long-Term Aging And Moisture Damage on the Performance of Asphalt Mixture Incorporating Warm Mix Additive <i>Ilık Karışım Katkısı Katılan Asfalt Karışımının Performansına Uzun Süreli Yaşlanma ve Nem Zararının Birleştirilmiş Etkilerinin Değerlendirilmesi</i>	77-95

Araştırma Makalesi / Research Article

Bor ve Bor Atığının İnşaat Yıkıntı Atığı ile Normal Beton Üzerindeki Etkileri

*¹Muhammed Fatih YENTİMUR, ²Tuba KÜTÜK-SERT, ³Sezai KÜTÜK

¹Recep Tayyip Erdoğan Üniversitesi, Mühendislik ve Mimarlık Fakültesi, İnşaat Mühendisliği Bölümü, Rize, Türkiye, muhammedfatih.yentimur@erdogan.edu.tr, ORCID ID: <http://orcid.org/0000-0003-0496-9065>

²Recep Tayyip Erdoğan Üniversitesi, Mühendislik ve Mimarlık Fakültesi, İnşaat Mühendisliği Bölümü, Rize, Türkiye, tuba.kutuk@erdogan.edu.tr, ORCID ID: <http://orcid.org/0000-0003-1747-9946>

³Recep Tayyip Erdoğan Üniversitesi, Turgut Kıran Denizcilik Fakültesi, Gemi Makineleri İşletme Mühendisliği Bölümü, Rize, Türkiye, sezai.kutuk@erdogan.edu.tr, ORCID ID: <https://orcid.org/0000-0002-0159-5953>

Geliş / Received: 24.05.2022

Kabul / Accepted: 01.11.2022

Öz

İnşaat yıkıntı atıklarının (İYA) depolama sahalarına döküm ücreti ve nakliye bedeli göz önüne alındığında ve ayrıca doğal kaynakların da az tüketilmesi açısından İYA'nın geri dönüşümünün sağlanması gerekmektedir. İYA'nın tekrar üretime katılmasıyla, beton üretimi için gerekli olan malzeme tasarrufu sağlanacaktır. Bu çalışmada, kentsel dönüşüm kapsamında oluşacak inşaat yıkıntı atıklarının (İYA) geri dönüşümü sağlanarak betonda kullanılabilirliği araştırılmıştır. %100 İYA, %100 normal agregası (NA) ve %50 İYA-%50 NA kullanılarak deneyler yapılmıştır. Bu numunelerden %50 İYA-%50 NA olanına %2, %5 bor ve %2, %5 bor atığı eklenerek, üretilen küp numunelerin basınç dayanımları ölçülmüştür. 28 günlük ortalama basınç dayanımı %50 İYA-%50 NA numunesi için 42,1 MPa, %2 bor atığı numunesi için 36,2 MPa, %5 bor atığı numunesi için 26,7 MPa, %2 bor katkısı numunesi için 35,1 MPa ve %5 bor katkısı numunesi için ise 30,7 MPa olarak bulunmuştur.

Anahtar kelimeler: Kentsel dönüşüm, İnşaat yıkıntı atığı, Bor, Beton, Basınç dayanımı

*¹Sorumlu yazar / Corresponding author

Bu makaleye atıf yapmak için

Yentimur, M., Kütük-Sert, T., Kütük, S., Hacimustafa, A., Kaya, E., Harbutoğlu, H. & Aktaş, S. (2022). Bor ve Bor Atığının İnşaat Yıkıntı Atığı ile Normal Beton Üzerindeki Etkileri. *Journal of Innovations in Civil Engineering and Technology (JICIVILTECH)*, 4(2), 47-60.

Effects of Boron and Boron Waste with Recycling Aggregate on Normal Concrete

Abstract

Construction debris wastes (CDW) need to be recycled, considering the cost of dumping construction debris to landfills and transportation costs, as well as less consumption of natural resources. With the re-joining of the construction debris waste in production, the material savings required for concrete production will be achieved. In this study, the recycling of construction debris wastes that will occur within the scope of urban transformation and its usability in concrete pavement were investigated. Experiments were carried out using 100% cleared CDW, 100% normal aggregate (NA), and 50% CDW-50% NA. Compressive strengths of cube samples produced by adding 2%, 5% boron and 2%, 5% boron waste to 50% CDW-50% NA of these samples were measured. The 28 -day average compressive strength was found to be 42.1 MPa for 50% CDW-50% NA sample, 36.2 MPa for 2% boron waste added sample, 26.7 MPa for 5% boron waste added sample, 35.1 MPa for 2% boron added sample and 30.7 MPa for 5% boron added sample.

Keywords: *Urban Transformation, Construction Debris Waste, Boron, Concrete, Compressive Strength*

1. Giriş

İnşaat ve yıkım faaliyetleri çevre için önemli bir tehdit oluşturmaktadır ve bunların olumsuz etkileri arasında atık üretimi, artan kirlilik, arazi bozulması ve kaynakların tükenmesi yer almaktadır (Lu & Tam, 2013). İnşaat endüstrisindeki son eğilim, enerji tüketimi, kirlilik, atık bertarafı ve küresel ısınma açısından çevresel etkiyi azaltmak için saf malzeme kullanımının yerini alabilecek alternatif yapı malzemelerinin kullanılmasıdır. Öte yandan, eski yapıların yıkılması ve inşaat faaliyetlerinden kaynaklanan atıklar tüm dünyayı endişelendirmektedir (Behera, Bhattacharyya, Minocha, Deoliya, & Maiti, 2014). Beton, temel olarak bağlayıcı malzemeler, su, agregalar ve katkıları gibi farklı bileşenlerden oluşan kompozit bir malzemedir. Bu bileşenler arasında agrega, toplam beton hacminin yaklaşık %60-75'ini kapladığı için çok önemli bir rol oynamaktadır (Kosmatka, Panarese, & Kerkhoff, 2002). Yıllık beton kullanımının 20 milyar ton olduğu düşünülmektedir (Mehta & Meryman, 2009). Bununla birlikte, inşaat yıkıntı atıkları, herhangi bir toplumda üretilen toplam katı atığın yaklaşık %10 ila %30'unu oluşturur (Li & Zang, 2013). Atık akışının önemli bir kısmı etkisizdir ve uygun şekilde yönetilirse yeniden kullanılabilir/geri dönüştürülebilir (Rao, Jha, & Misra, 2007). Kentsel dönüşüm kapsamında yıkılan bina atıklarının, çevresel faktörler de göz önüne alınarak kullanılması ihtiyacı doğmuştur. İnşaat atıkları, insan yaşamının ayrılmaz bir parçası olan başlıca çevre kirleticilerinden biridir.

Günümüzde bilimin ilerlemesi ile üretim teknolojisi ve katı atık yönetimi çok değişmiştir (BandehLou, Parvishi, & Kheradranjbar, 2016). Türkiye genelinde konut talebi, arzı fazlasıyla geçmiş bulunmaktadır. Bu talebin zamanında karşılanamaması, çarpık kentleşmeyi ve depreme karşı dayanımı düşük yapıları beraberinde getirmektedir. Gelişmekte olan ülkelerdeki temel problemlerden biri olan gecekondulaşma, deprem anında çok büyük sorunlara neden olmaktadır.

Kentsel dönüşüm ile yıkılan yapılarda atık malzeme olarak ortaya çıkan molozlar geri dönüştürülebilir bir materyaldir. Molozlar, hammadde ve yapı malzemesi tedariki açısından, beton üretim aşamasında agrega ve yol inşaatlarının altyapısında dolgu malzemesi olarak kullanılabilir. Ayrıca, inşaat yıkıntı atıklarının uygun şekilde geri dönüştürülmesi konusunda da önemli bir araçtır. Beton üretilirken kullanılan doğal agrega yerine molozların kullanılması ile istenilen beton dayanımının sağlandığı görülmüştür (Abbas, Fathifazl, Isgor, Razaqpur, Fouriner, Foo, 2006). Öte yandan, yıkılacak yapının diğer materyalleri de geri dönüşüm yolu ile farklı şekillerde değerlendirilebilir.

Doğal agregalar; çeşitli yollarla elde edilebilir. Bu yollardan bazıları; nehir yatakları, denizler ve taş ocakları olarak sıralanabilir. Tüm madenler içinde dünya genelinde en yüksek pay %58 ile agrega üretimidir (agrega kullanımı Avrupa'da yıllık 7 ton/kişi ve Türkiye'de 4 ton/kişi). Agregaya kaynaklarının yüksek miktarlarda tüketiminden dolayı, ilerleyen senelerde dünyanın ekolojik olarak negatif yönde etkileneceği ve bu

kaynakların tükenme riskinde olduğu düşünülmektedir (Öztürk, Çelikkol, & Erkan, 2007). Fazla miktarda ihtiyaç olan agrega kaynaklarının tüketilmesi ve inşaat yıkıntı atıklarının (İYA) çevreye verdiği zararlar, geri kazanılmış agreganın kullanılmasını zorunlu kılmaktadır. Geri kazanılmış beton agregalarının ve içinde kullandıkları betonun özelliklerini belirlemek amacıyla pek çok araştırma yapılmıştır. Bunun yanı sıra, dünyada ticari öneme sahip bor yatakları Türkiye, Rusya, Güney Amerika ve ABD'dedir. Türkiye 3,3 milyar ton ile dünya bor rezervinin %73'üne ev sahipliği yapmaktadır. Başka bir ifadeyle, yıllık tüketiminin kabaca 4 milyon ton (+/-%10) olduğu hesaba katılırsa, bu rezerv 1.000 yıl kadar yetecek düzeydedir. Bununla birlikte dünya bor pazarındaki durum gün geçtikçe yükselmektedir ve 2020 yılında bor pazar payı %57 değerine ulaşmıştır (Eti Maden, 2020).

Türkiye'de bulunan ticari değere sahip bor mineralleri, tinkal ($\text{Na}_2\text{B}_4\text{O}_7 \cdot 10\text{H}_2\text{O}$), kolemanit ($\text{Ca}_2\text{B}_6\text{O}_{11} \cdot 5\text{H}_2\text{O}$) ve üleksittir ($\text{NaCaB}_5\text{O}_9 \cdot 8\text{H}_2\text{O}$) (Bayca, Batar, Sayın, Solak, & Kahraman, 2008; Batar, Köksal, Yersel, 2009). Bor minerallerinin içindeki B_2O_3 (bor trioksit) oranına "tenör" adı verilmektedir. Bor madenlerinin değeri, içindeki B_2O_3 oranı ile ölçülmekte ve yüksek miktarda bu orana sahip olanlar daha değerli kabul edilmektedir (Buluttekin, 2008). Yüksek tenördeki bor cevherleri ekonomik olarak çıkarılmakta ve işlenmektedir (Kütük-Sert, 2016; Kütük & Kütük-Sert, 2020).

Son zamanlarda artan çevre bilinci madencilik sektöründe de kendisini hissettirmiş, madencilik faaliyetleri sonucu oluşan atıkların çevreye zarar

vermeden bertaraf edilmesi hususunda çeşitli yönetmelikler ve standartlar getirilmiştir. Bor atıklarının uygun yöntemlerle çeşitli sektörlerde değerlendirilmesi sonucunda;

- Atıkların stoklanmasından doğan sorunlar ve stoklama maliyeti azalacak,
- Çevreyi kirleten unsurlar asgari düzeye indirilecek,
- Bor atıklarının değerlendirilmesi sonucu üretilen yeni ürünler, ülke ekonomisine ek kazanç sağlayacaktır (Kütük-Sert & Kütük, 2013).

Son yıllarda bor minerallerinin çimento katkısı olarak kullanımı üzerine çeşitli çalışmalar yapılmış ve yapılmaya devam etmektedir (Kütük-Sert, Kara & Kütük, 2020). Türkiye'deki bor rezervleri düşünüldüğünde, bu çalışmaların ülkemiz için önemi kat ve kat daha fazladır.

Bor atığı katkılı killerin seramik sektöründe frit, sır ve masse hazırlanmasında kullanılabilirliği kanıtlanmıştır (Sönmez, Özdağ, Özler, & Sümer, 1993). Bu çalışmanın amacı, sınırlı kaynakları tüketmek yerine, atıkların değerlendirilmesini sağlamaktır. Betonda hem İYA hem de bor atıklarının birlikte kullanımı ile ilgili literatürde herhangi bir çalışmaya rastlanmamıştır. Bu yüzden, bu çalışmada İYA ve bor atıkları farklı oranlarda betona katkı yapılmış; beton numunelerinin basınç dayanımları ölçülmüş ve tartışılmıştır.

2. Materyal ve Yöntem

Bu çalışmada, inşaat yıkıntı atığı (İYA) ve normal agrega (NA) olmak üzere iki çeşit agrega kullanılmıştır. Bunlarla yapılan karışımlara belirli oranlarda bor minerali ve bor atığı eklenerek deney

tabi tutulmuştur. Bu deneylerde, İYA olan beton molozlarının elle (çekiç yardımıyla) kırılıp elenerek 0-4 mm ve 4-16 mm boyutunda ince ve iri İYA üretilmiştir (Li X. , 2008).

Normal agregra grupları belirli oranlarda azaltılarak yerine inşaat yıkıntı atığı ilave edilmiş ve C25/30 beton sınıfında beton numuneleri üretilmiştir. Karışımlarda iri ve ince İYA ile birlikte kullanılarak %50 ağırlıkça ikame edilmiştir. Beton numuneleri laboratuvar ortamında teste tabi tutularak basınç dayanımları belirlenmiştir. Beton üretiminde bağlayıcı olarak Muş Yurtçim Portland çimentosu (TS-EN 197-1;2012 CEM IV/B (P) 32,5 R) ve karışım suyu olarak şebeke suyu kullanılmıştır. Katkı olarak %2 ve %5 oranlarında bor minerali ve bor atığı kullanılmıştır. Su/çimento oranı 0,39 olan, katkılı, İYA agregalı beton ve normal agregalı beton serileri dökülmüştür.

Yapılan çalışmalar, arazi çalışmaları ve laboratuvar ortamında yapılan deneysel çalışmalar olmak üzere ikiye ayrılmaktadır. Arazi çalışmaları;

- İnşaat yıkıntı atıklarının toplanması,
- Alınan atık beton kütlelerinden karot numunelerinin alınması,
- Toplanan beton kütlelerinin elle (çekiç yardımıyla) kırılması,
- Kırılan betondan iri ve ince inşaat yıkıntı atığının elde edilmesidir.

Laboratuvar ortamında yapılan deneysel çalışmalar ise;

- Elek analizi deneyi ile inşaat yıkıntı atığının tane büyüklüğü dağılımının belirlenmesi,
- İYA birim hacim ağırlığı ve su emmesinin belirlenmesi,

- %100 NA, %100 İYA, %50 İYA – %50 NA, %50 İYA – %50 NA – %2 Bor, %50 İYA – %50 NA – %5 Bor, %50 İYA – %50 NA – %2 Bor Atığı, %50 İYA – %50 NA – %5 Bor Atığı olan karışım oranlarında 6'şar adet beton numunelerinin üretilmesi; 7 ve 28 gün kür havuzunda bekletilmesi işlemi,
- Farklı karışım oranlarındaki numunelerin basınç dayanım testidir (TS 802, 2016).

İYA ve NA numunelerinin karışım hesabı, TS 802 – Beton Karışım Tasarımı Hesap Esasları dikkate alınarak tasarlanmıştır (TS 802, 2016).

İYA ve NA ile oluşturulacak olan beton numunelerinin karışım hesabında çökme değeri (slump değeri) 30 mm alınmıştır.

İYA ile üretilecek beton numuneleri için elde edilen agreganın maksimum tane büyüklüğü 16 mm olarak belirlenmiştir. Betonun karışım suyu miktarı, agreganın büyük tane büyüklüğüne, betonun kıvamına, betonun içerisinde kullanılacak olan kimyasal katkıya ve hava sürükleyici katkıya bağlı olarak değişiklik göstermektedir. Beton üretimi için gerekli olan yaklaşık karışım suyu miktarı, TS 802'den betonun çökmesi ve en büyük agreganın tane büyüklüğüne göre verilen referans değerler göz önünde bulundurularak belirlenmiştir (TS 802, 2016). 30 mm çökme değerine sahip beton için inşaat yıkıntı atığının en büyük agreganın tane büyüklüğü 16 mm olduğundan dolayı, karışım suyu miktarı 166 kg/m³ olarak belirlenmiştir. Ayrıca betona ilave olarak %2 ile %5 oranında bor (kolemanit minerali) ve %2 ile %5 oranında bor atığı kullanılmıştır.

Tablo 1. Bor mineralinin oksitli bileşen analizi

Bileşen	Kolemanit (% ağırlıkça)
	C-75 μm
B ₂ O ₃	40 \pm 0,50
B ₂ O ₃ (Bu çalışma için)	38,65 \pm 1,00
CaO	27,00 \pm 1,00
SiO ₂	4,00-6,50
SO ₄	0,60 maksimum
As	35 ppm maksimum
MgO	3,00 maksimum
SrO	1,50 maksimum
Al ₂ O ₃	0,40 maksimum
Na ₂ O	0,35 maksimum
Fe ₂ O ₃	0,08 maksimum
Nem	1,00 maksimum

Kullanılan bor mineralinin kimyasal analizi Tablo 1’de verilmiştir (Kütük, 2017). Şekil 1, Şekil 2 ve Şekil 3’te sırasıyla; inşaat yıkıntı atıkları, toplanan beton kütlelerinin çekiç yardımıyla kırılması ve sonucunda elde edilen İYA gösterilmiştir.

**Şekil 1.** İnşaat yıkıntı atıkları**Şekil 2.** Toplanan beton kütlelerinin çekiç yardımıyla kırılması**Şekil 3.** Elde edilen inşaat yıkıntı atığı

Arazi çalışmaları kısmında atık beton kütlelerinden karot numunelerinin alınması Şekil 4’te gösterilmiştir.



Şekil 4. Atık beton kütlelerinden karot numunelerinin alınması

İYA ve NA ile üretilcek olan beton numunelerinin bileşenleri belirlenen oranda tartılarak önceden nemlendirilmiş betoniye konulmuştur. Önce Şekil 5'te görüldüğü üzere iri ve ince agregalar konulup 1-2 dakika karıştırılmıştır. Daha sonra çimento, bor ve bor atığı eklenip 2-3 dakika daha karıştırılmaya devam etmiştir. Ardından su eklenerek 3-5 dakika daha karıştırılan beton, Şekil 6'da görülen son halini almıştır.



Şekil 5. Kuru malzemelerin betoniyerde karıştırılması



Şekil 6. Beton karışımı

Karıştırma işleminin tamamlanmasının ardından daha önceden temizlenmiş ve yağlanmış olan beton numune kalıplarına beton karışımı Şekil 7'de görüldüğü gibi yerleştirilmiştir.



Şekil 7. Kalıplara karışım betonunu yerleştirilmesi

Verilen karışım olanlarında toplamda 42 adet 15x15x15 cm boyutunda beton küp numune üretilmiştir. Üretilen beton küp numuneler 7 gün ve 28 gün kür havuzunda bekletilmiştir. Kür havuzundan çıkarılan küp numuneler üzerinde basınç dayanım deneyi uygulanmıştır.

3. Bulgular ve Tartışma

Çalışmada kullanılan NA ve İYA agregasına elek analizi yapılarak 1 no'lu

mıcır, 2 no'lu mıcır, kırma kum ve kum boyutlarına ayrılmıştır (TS EN 932-1, 1997). Her bir boyut için birim hacim ağırlıkları ve ağırlıkça su emme oranları

hesaplanmıştır. Sonuçlar Tablo 2 ve Tablo 3'te verilmiştir.

Tablo 2. Normal agreganın birim hacim ağırlık ve su emme değerleri

	1 no'lu mıcır	2 no'lu mıcır	Kırma kum	Kum
Birim Hacim Ağırlığı	2,65	2,66	2,82	2,00
Su Emme	1,23	0,80	5,13	8,17

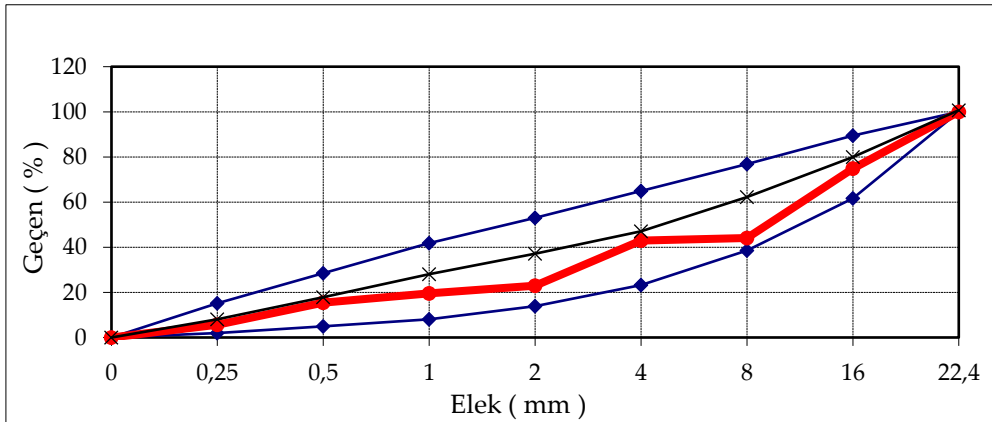
Tablo 3. İnşaat yıkıntı atığı birim hacim ağırlık ve su emme değerleri

	1 no'lu mıcır	2 no'lu mıcır	Kırma kum	Kum
Birim Hacim Ağırlığı	2,40	2,35	0,54	0,40
Su Emme	7,40	9,10	11,40	26,1

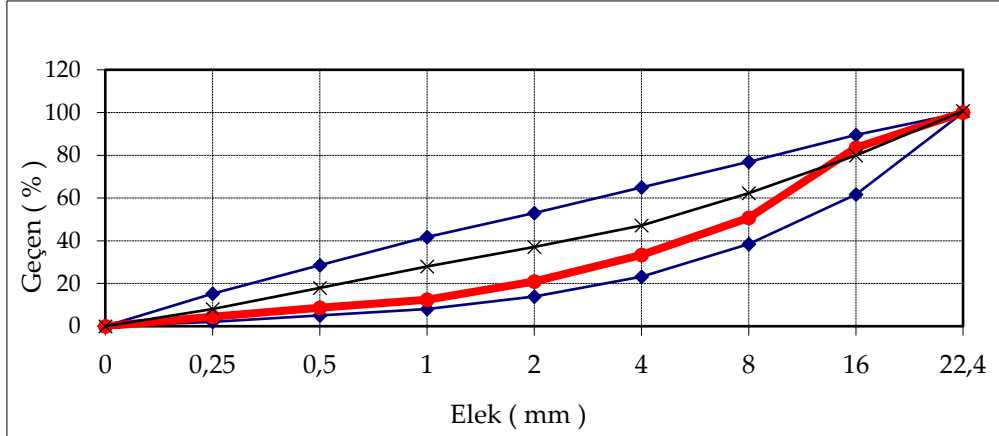
3.1. Agreganın Tane Büyüklüğü Dağılımı

İri ve ince agregalara ait numunelerin dane büyüklüklerine göre dağılımı elek analizi sonucunda belirlenmiştir. Kullanılan agregaların maksimum dane boyutu 16 mm olarak bulunmuştur. İri ve ince agreganın dane dağılımları için agreganın dağılımını belirleyebilmek amacıyla, belirli yüzdelere denenecek beton agregaları standartları TS 706 EN

12620+A1'deki maksimum dane büyüklüğü 16 mm olan eğrilere ait alt (A), orta (B) ve üst sınırlara (C) uygun, özellikle alt sınır ile orta arasında yer alacak şekilde karışık agreganın granülometrisi ayarlanmıştır (TS 706 EN 12620+A1, 2009). Şekil 8'de normal agreganın için, Şekil 9'da ise inşaat yıkıntı atığı için granülometri eğrisi sunulmuştur.



Şekil 8. Normal agreganın granülometri eğrisi

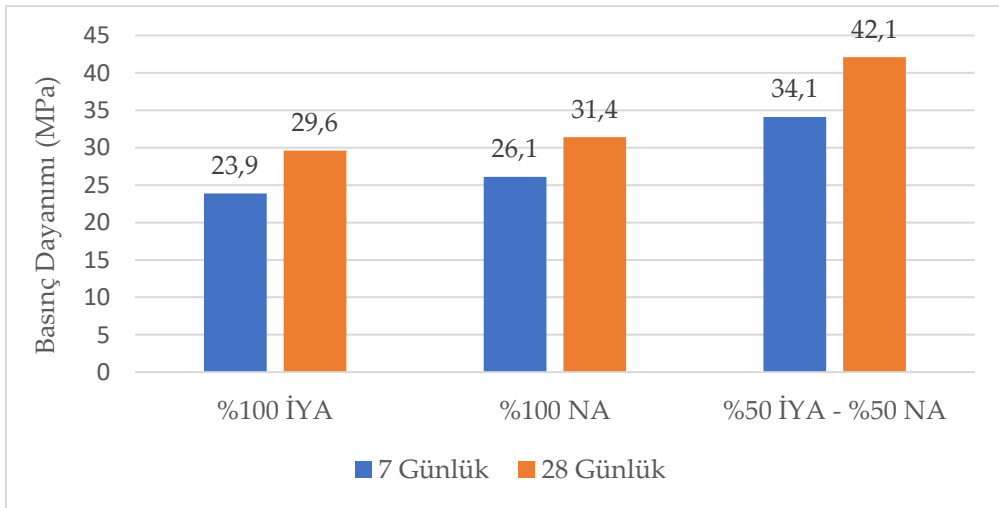


Şekil 9. İnşaat yıkıntı atığı granülometri eğrisi

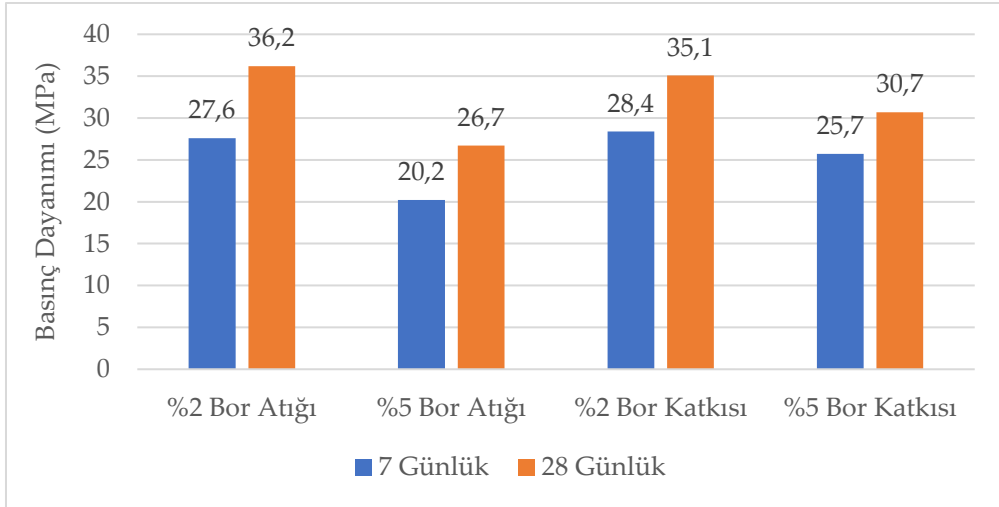
3.2. Beton Numunelerinin Basınç Dayanımı

Şekil 10'da bor atığı ve bor katkısı olmayan, %100 İYA, %100 NA ve %50 İYA-%50 NA beton küp numunelerine ait 7 günlük ve 28 günlük ortalama basınç dayanımı değerleri verilmiştir. Şekil 11'de ise %50 İYA-%50 NA ilave

olarak sırasıyla %2 bor atığı, %5 bor atığı, %2 bor katkılı, %5 bor katkılı beton küp numunelerine ait 7 günlük ve 28 günlük ortalama basınç dayanımı değerleri verilmiştir.



Şekil 10. Bor Katkısız Beton Numunelerinin Basınç Dayanımı Değerleri



Şekil 11. %50 İYA – %50 NA ve Bor ile Bor Atığı Katkılı Beton Numunelerinin Basınc Dayanımı Değerleri

Üretilen beton numuneleri C25/30 beton sınıfında olduğundan dolayı, küp numunelerin 28 günlük dayanımlarının 30 MPa değeri ile kıyaslaması yapılabilir:

- %100 İYA ile üretilen betonun ortalama basınç dayanımı 29,6 MPa ile bu değer hemen hemen karşılandığı,
- %100 NA ile üretilen betonun ortalama basınç dayanımı 31,4 MPa ile bu değer karşılandığı,
- %50 İYA-%50 NA ile üretilen betonun ortalama basınç dayanımı 42,1 MPa ile bu değer fazlasıyla üstünde olduğu,
- %50 İYA-%50 NA ile üretilen betona %2 bor atığı eklendiğinde, ortalama basınç dayanımı 36,2 MPa ile bu değer karşılandığı,
- %50 İYA-%50 NA ile üretilen betona %5 bor atığı eklendiğinde, ortalama basınç dayanımı 26,7 MPa ile bu değer altında kaldığı,
- %50 İYA-%50 NA ile üretilen betona %2 bor katkı olarak eklendiğinde,

ortalama basınç dayanımı 35,1 MPa ile bu değer karşılandığı,

- %50 İYA-%50 NA ile üretilen betona %5 bor katkı olarak eklendiğinde, ortalama basınç dayanımı 30,7 MPa ile bu değer karşılandığı anlaşılmıştır.

Bu verilerden özetle ifade edilirse, C25/30 beton sınıfında hedef dayanımı 30 MPa'a ulaşılması istendiği için şu yorum yapılabilir:

%100 NA, %50 İYA-%50 NA, %50 İYA-%50 NA-%2 bor atığı, %50 İYA-%50 NA-%2 bor katkısı, %50 İYA-%50 NA-%5 bor katkısı ile üretilen beton numunelerinde amaç dayanıma ulaşırken; %100 İYA ve %50 İYA-%50 NA-%5 bor atığı ile üretilen beton numunelerinde ise amaçlanan dayanım elde edilememiştir.

En yüksek basınç dayanımı 42,1 MPa ile %50 İYA-%50 NA beton numunesinde saptanmıştır. Bu yüksek değer İYA'daki yapışık olan çimento kalıntılarında kaynaklandığı düşünülmektedir. Bu kayda değer

sonuç, çimento tüketiminde tasarruf sağlayabilecektir.

Beton numunelerinin 28 günlük basınç dayanımları, %100 NA ile karşılaştırılmış ve aşağıdaki sonuçlar tespit edilmiştir:

- %100 İYA ile üretilen betonun basınç dayanım değerinin %100 normal agregaya göre %5,73 daha az olduğu,
- %50 İYA-%50 NA-%5 bor atığı katkısı ile üretilen betonun basınç dayanım değerinin %100 normal agregaya göre %11,97 daha az olduğu,
- %50 İYA-%50 NA-%5 bor katkısı ile üretilen betonun basınç dayanım değerinin %100 NA ile üretilen betona göre %2,23 daha az olduğu,
- %50 İYA-%50 NA ile üretilen betonun basınç dayanım değerinin %100 normal agregaya göre %34,1 daha fazla olduğu,
- %50 İYA-%50 NA-%2 bor atığı katkısı ile üretilen betonun basınç dayanım değerinin %100 normal agregaya göre %15,29 daha fazla olduğu,
- %50 İYA-%50 NA-%2 bor katkısı ile üretilen betonun basınç dayanım değerinin %100 normal agregaya göre %11,78 daha fazla olduğu görülmüştür.

Ayrıca bor ve bor atığı katkıları kullanılarak hazırlanan numunelerin dayanım sonuçları kendi içerisinde mukayese edildiğinde, bor katkılı betonların basınç dayanımlarının ortalaması (32,9 MPa) bor atığı katkılı betonların basınç dayanımlarının ortalamasından (31,45 MPa) biraz daha büyük olduğu belirlenmiştir.

Elde edilen bu sonuçlar literatürde araştırılmıştır. Durmuş vd. tarafından yapılan bir çalışmada, iri geri dönüşüm beton agregası oranı arttıkça betonun basınç dayanımının azaldığı belirlenmiştir. Yani, basınç dayanımı, %0 İGDBA kullanımında 43,92 MPa iken %100 İGDBA kullanımında 29,90 MPa'a düşmüştür (Durmuş, Şimşek, & Dayı, 2009). Demirel ve Şimşek tarafından yapılan bir çalışmada, atık beton geri dönüşüm agregası oranı yükseldikçe betonun basınç dayanımının düştüğü tespit edilmiştir. Başka bir deyişle, basınç dayanımı en yüksek %10 iri GDA kullanımında 36 MPa iken, en düşük %50 ince GDA kullanımında 26 MPa olarak bulunmuştur (Demirel & Şimşek, 2015). Kadiroğlu vd. geri dönüşümden elde edilen betonların kırılmasıyla oluşturulan agregalar, geri dönüşümlü agregaya (GDA) ve inşaat moloz atıkları (İMA) ile ilgili bir çalışma yapmıştır. Basınç dayanımının GDA oranının artmasıyla azaldığı saptanmıştır. Bununla birlikte İMA oranının %15'lere ulaşmasıyla basınç dayanımının azaldığı, tam tersine İMA oranının %25 olmasıyla basınç dayanımının yükseldiği görülmüştür. İMA'daki yükselişin nedeni, düşük klor iyon geçirimsizliği değerlerine atfedilmiştir (Kadiroğlu, Öz, Tezcan, & Kuru, 2017). Bu çalışmada, hem bor atığı hem de bor ilavesinin %2'den %5'e çıkmasıyla betonun basınç dayanımının azaldığı bulunmuştur. Kara vd. tarafından yapılan çalışmalarda, bu sonuca benzer sonuçlar elde edilmiştir: Bor (kolemanit) ikamesinin %3'e kadar betonun basınç dayanımını ve aşınma dayanımını iyileştirdiği, fakat daha yüksek oranlarda kötüleştirdiği tespit edilmiştir

(Kara, Kütük-Sert & Kütük, 2020; Kütük-Sert, Kara & Kütük, 2020).

4. Sonuçlar

Bu çalışmada, atık beton kütleleri el ile kırılarak (çekiç yardımıyla) inşaat yıkıntı atığı elde edilmiştir. Sonrasında beton karışımına %50 oranında inşaat yıkıntı atığı ikame edilerek üretilen beton numuneleri üzerinde basınç dayanımı deneyi yapılmıştır. Ayrıca bu numunelere %2 ve %5 oranlarında bor ve bor atığı ilave edilerek bu katkıların beton dayanımına etkisi gözlemlenmiştir. Deneylerden elde edilen verilerden aşağıdaki sonuçlara ulaşılmıştır:

- Basınç dayanım değerlerinin en büyüğüne 42,1 MPa ile %50 inşaat yıkıntı atığı-%50 normal agregaya ile üretilen beton sahip iken, en küçüğüne ise 26,7 MPa ile %50 inşaat yıkıntı atığı-%50 normal agregaya-%5 bor atığı ilavesi ile üretilen beton sahiptir.
- Atıkların değerlendirilmesi, çevre kirliliğinin azaltılması, normal agregaya kullanımından ve çimento miktarından tasarruf sağlanması ve beton dayanımı açısından inşaat yıkıntı atığı agregalarının belli oranlarda kullanılabilmesi düşünülmektedir.

Teşekkür

Yazarlar, deneylerin yapılmasına yardımcı olan Öğr. Gör. M. Selçuk GÜNER'e, bor minerallerin temininde Eti Maden İşletmeleri Genel Müdürlüğü'ne, İnşaat Mühendisliği Bölümü Bitirme Tezi kapsamında çalışmayı yürüten öğrencilerimiz Atilla

HACIMUSTAFALOĞLU, Emine KAYA, Halil HARBUTOĞLU ve Selin AKTAŞ'a teşekkür etmektedir.

5. Kaynaklar

- Abbas, A., Fathifazl, G., Isgor, O. B., Razaqpur, A. G., Fouriner, B., & Foo, S. (2006). Environmental benefits of green concrete. (s. 1-8). *Climate Change Technology*.
- BandehLou, A. K., Parvishi, A., & Kheradranjbar, M. (2016). Study of Construction Debris Waste and the Role of Recycling to Protect the Environment. *International Journal of Advanced biotechnology and Research*, 1748-1754.
- Batar, T., Köksal, S., & Yersel, E. (2009). Atık bor, atık kağıt ve perlit katkılı sıva malzemesinin üretimi ve karakterizasyonu. *Ekoloji*, 45-53.
- Bayca, S. U., Batar, T., Sayın, E., Solak, O., & Kahraman, B. (2008). The influence of coal ash and tincal (boron mineral) additions on the physical properties and microstructures of ceramic bodies. *Journal of Ceramic Processing Reserch*, 118-122.
- Behera, M., Bhattacharyya, S. K., Minocha, A. K., Deoliya, R., & Maiti, S. (2014). Recycled aggregate from C&D waste & its use in concrete – A breakthrough towards sustainability in construction sector: A review. *Construction and Building Materials*, 501-516.
- Buluttekin, B. (2008). Bor maden ekonomisi: Türkiye'nin dünya bor piyasasındaki yeri. 2. Ulusal İktisat Kongresi. İzmir: Dokuz Eylül Üniversitesi, İktisat Bölümü.
- Demirel, C., & Şimşek, O. (2015). Erken yaşdaki atık betonların geri dönüşüm agregası olarak beton üretiminde kullanılabilirliği ve sürdürülebilirlik açısından

- incelenmesi. *Düzce Üniversitesi Bilim ve Teknoloji Dergisi*, 226-235.
- Durmuş, G., Şimşek, O., & Dayı, M. (2009). Geri dönüşümlü iri agregaların beton özelliklerine etkisi. *Gazi Üniversitesi Mühendislik ve Mimarlık Fakültesi Dergisi*, 183-189.
- Eti Maden. (2022). 2020 Yılı Faaliyet Raporu. Ankara: Eti Maden İşletmeleri Genel Müdürlüğü. https://www.etimaden.gov.tr/storage/2021/Etimaden_2020_Faaliyet_Raporu.pdf adresinden alındı
- Kadiroğlu, İ., Öz, E., Tezcan, O., & Kuru, E. B. (2017). Geri dönüşümlü agreganın beton üretiminde kullanılabilirliği. *Hazır Beton*, 86-94.
- Kara, C., Kütük-Sert, T., & Kütük, S. (2020). Öğütülmüş kolemanit içeren betonlarda sodyum klorür etkisi. *Düzce Üniversitesi Bilim ve Teknoloji Dergisi*, 499-510.
- Kosmatka, S. H., Panarese, W. C., & Kerckhoff, B. (2002). Design and control of concrete mixtures. Skokie: Portland Cement Association.
- Kutuk-Sert, T. (2016). Stability analyses of submicron-boron mineral prepared by mechanical milling process in concrete roads. *Construction and Building Materials* 121, s. 255-264.
- Kütük, S. (2017). Öğütülmüş nano boyutlu kolemanit mineralinin elementel ve kristal yapı özellikleri. *Erzincan Üniversitesi Fen Bilimleri Enstitüsü Dergisi*, 303-313.
- Kütük-Sert, T. (2020). An examination of nanoparticle colemanite mineral added warm mix asphalt. *Construction and Building Materials* 243 118252
- Kütük-Sert, T., & Kütük, S. (2013). Physical and Marshall Properties of Borogypsum Used as Filler Aggregate in Asphalt Concrete. *Journal of Materials in Civil Engineering*, 266-273.
- Kütük-Sert, T., Kara, C., & Kütük, S. (2020). Öğütülmüş kolemanit minerali ikameli beton yollardaki aşınma kaybının araştırılması. *Afyon Kocatepe Üniversitesi Fen ve Mühendislik Bilimleri Dergisi*, 287-295.
- Li, X. (2008). Recycling and reuse of waste concrete in China: Part I. Material behaviour of recycled aggregate concrete. *Resources, Conservation and Recycling*, 36-44.
- Li, Y., & Zang, X. (2013). Web-based construction waste estimation system for building construction projects. *Automation in Construction*, 142-156.
- Lu, W., & Tam, V. W. (2013). Construction waste management policies and their effectiveness in Hong Kong: A longitudinal review. *Renewable and Sustainable Energy Reviews*, 214-223.
- Mehta, P. K., & Meryman, H. (2009). Tools for reducing carbon emissions due to cement consumption. *Structure Magazine*, 11-15.
- Öztürk, Ö., Çelikkol, M., & Erkan, M. (2007). Türkiye Agregası Sektör Raporu.
- Rao, A., Jha, K. N., & Misra, S. (2007). Use of aggregates from recycled construction and demolition waste in concrete. *Resources, Conservation and Construction and Demolition Waste in Concrete*, 71-81.
- Sönmez, E., Özdağ, H., Özler, A., & Sümer, G. (1993). Kırka Boraks İşletmesi atık kollarının seramik endüstrisinde kullanılabilirliğinin araştırılması. Türkiye XIII. Madencilik Kongresi (s. 561-566). İstanbul: TMMOB Maden Mühendisleri Odası.
- TS 706 EN 12620+A1. (2009, Nisan 28). Beton Agregaları. Ankara.
- TS 802. (2016). Beton Karışım Tasarımı Hesap Esasları.

- TS EN 932-1. (1997, Şubat 25). Agregaların genel özellikleri için deneyler-Kısım 1 numune alma metotları. Ankara.
- TS-EN 197-1:2012. (2012). Çimento- Bölüm 1: Genel çimentolar- Bileşim, özellikler ve uygunluk kriterleri.

Araştırma Makalesi / Research Article

**Buckling of Square and Circular Perforated Square Plates
under Uniaxial Loading**

*¹Fethullah USLU, ²Mustafa Halûk SARAÇOĞLU, ³Uğur ALBAYRAK

¹Kütahya Dumlupınar University, Faculty of Engineering, Department of Civil Engineering, Kütahya, Türkiye, fethullah.uslu@dpu.edu.tr, ORCID ID: <http://orcid.org/0000-0001-8057-5119>

²Kütahya Dumlupınar University, Faculty of Engineering, Department of Civil Engineering, Kütahya, Türkiye, mhaluk.saracoglu@dpu.edu.tr, ORCID ID: <http://orcid.org/0000-0003-3842-5699>

³Eskişehir Osmangazi University, Faculty of Engineering and Architecture, Department of Civil Engineering, Eskişehir, Türkiye, albayrak@ogu.edu.tr, ORCID ID: <http://orcid.org/0000-0001-7326-3213>

Geliş / Recieved: 18.10.2022;

Kabul / Accepted: 10.11.2022

Abstract

This paper aims to investigate the critical buckling loads of uniaxially loaded simply supported square thin plates with central circular and square holes in terms of some parameters like hole shapes, slenderness ratios and total hole areas. In this study, buckling analyses of perforated plates with different hole shapes of perforation and slenderness ratios were carried out. For this purpose, plate models with seven different total hole areas were examined together with the non-perforated plate. The total hole area ratios in the models are 0.79%, 3.14%, 7.07%, 12.57%, 19.63%, 28.27% and 38.48%, respectively. The total hole areas of the models with square holes are arranged to be the same as the models with circular holes to compare the results among circular and square perforated plates properly. The models were established by using the finite-element (FE) software ANSYS using Shell-181 elements which are 4-node structural shell elements. The comparisons on critical buckling loads between square and circular perforated results show that the buckling load for the plates with square holes is higher than for the plates with circular holes.

Keywords: Buckling, Perforated plates, Finite element, Square perforated, Circular perforated

*¹Sorumlu yazar / Corresponding author

Bu makaleye atıf yapmak için

Uslu, F, Saraçoğlu, M. H. & Albayrak, U. (2022). Buckling of Square and Circular Perforated Square Plates under Uniaxial Loading. *Journal of Innovations in Civil Engineering and Technology (JICIVILTECH)*, 4(2), 61-75.

Tek Eksenli Yükleme Altındaki Kare ve Dairesel Delikli Kare Plakların Burkulması

Öz

Bu makale, merkezi dairesel ve kare deliklere sahip tek eksenli yüklü basit mesnetli kare ince plakların kritik burkulma yüklerini delik şekilleri, narinlik oranları ve toplam delik alanları gibi bazı parametreler açısından incelemeyi amaçlamaktadır. Bu çalışmada, farklı delik şekillerine ve narinlik oranlarına sahip delikli plakların burkulma analizleri yapılmıştır. Bu amaçla boşluksuz plak ile beraber yedi farklı boşluk oranına sahip plak modelleri incelenmiştir. Modellerdeki boşluk oranları sırasıyla %0.79, %3.14, %7.07, %12.57, %19.63, %28.27 ve %38.48 şeklindedir. Dairesel ve kare delikli plaklar arasındaki sonuçları doğru bir şekilde karşılaştırabilmek için kare delikli modellerin toplam delik alanları, dairesel delikli modellerle aynı olacak şekilde düzenlenmiştir. Modeller, kütüphanesinde bulunan 4 düğüm noktalı yapısal kabuk elemanı olan Shell-181 elemanları kullanılarak sonlu elemanlar yazılımı ANSYS ile analiz edilmiştir. Elde edilen sonuçlar, aynı boşluk alanına sahip kare delikli plakaların burkulma yüklerinin dairesel delikli plakalara göre daha yüksek olduğunu göstermiştir.

Anahtar kelimeler: Burkulma, Delikli plaklar, Sonlu eleman, Kare delik, Dairesel delik.

1.Introduction

Perforated plates are used in many engineering areas as a structural member and are subjected to a wide variety of loads. One of these loads is the buckling load which was acting in-plane uniaxial compressive to these members. Buckling behavior is often encountered in such structures and commonly generates large deformations. Therefore, buckling design for perforated plates used as the main structural member is gaining considerable importance in the structural designs.

In this sense, although there are studies on perforated plates, there has not been much research on buckling and there are few studies on this subject in the literature. There were also studies about perforated rectangular and square plates subjected to various loads as lateral bending and inplane tension loads with different boundary conditions (Albayrak & Saraçoğlu, 2016; Saraçoğlu & Albayrak, 2018; Saraçoğlu et al., 2020; Saraçoğlu et al., 2021, Karakaya, 2022). Narayanan and Avanesian (1984), investigated stability of plates with cut-outs plates under shear by using finite element method. They computed buckling coefficient for simply and fixed supported plates containing various shaped cut-outs. After the calculations they suggested a formula for the use of practical engineers. Brown, presented elastic stability analyses of perforated plates with different aspect ratios for concentrated loading. He emphasizes in his study that some simple modifications to the boundary conditions and geometry of the plate affect the critical

load of the plate majorly (Brown, 1990). Shakerley and Brown (1996), studied buckling of square eccentrically positioned perforated plates with fully fixed and simply supported boundaries. They explained the effect of longitudinal or lateral slots and the location of perforations to the critical buckling load in their study. Shanmugam et al. (1999) have proposed critical loads for the design of perforated plates with different boundary conditions and different shapes of openings which are subject to uni-axial and bi-axial in-plane compressive loadings for design in their study. El-Sawy et al. (2004) have investigated the buckling stress of circular perforated rectangular and square plates subjected to uniaxial loadings. By using the finite element method effects of various parameters have been determined in their study. Maiorana et al. (2008) have investigated the stability of perforated plates with rectangular and circular holes under localized symmetric loads. Kömür and Sönmez (2008), were studied the stability of rectangular plates with different perforations and loading cases, different normalized hole sizes, and aspect ratios by using finite element software program ANSYS. Rezaeepazhand and Sabori (2008), were studied the damaged metallic perforated square plates and they conducted finite element codes for numerical studies. Maiorana et al. (2009) were were developed some numerical non-linear analyses for perforated plates with eccentric holes in their parametric study. In perforated plates, Komur (2011) selected elliptical holes as a different geometrical shape and he

investigates the effect of some parameters on buckling behavior. Seifi et al. (2017) were studied the global buckling behavior of reinforced perforated plates experimentally and numerically. Al-Amar and Al-Araji (2017) were investigated the buckling of perforated and unperforated stiffened plates under uniaxial compressive load. Yanli et al. (2019) investigated the buckling behavior of perforated plates under bending by using finite element software and a practical formula was proposed for the coefficient of buckling. Soares et al., (2019) studied about the buckling of perforated thin and thick plates. Investigated plates were considered with the simply supported boundary condition and loaded with uni axial in-plane loads. And also they compare the results with the literature. Soleimani et al. (2020) studied the buckling and vibration of perforated plates made with composite materials under thermal loads and they suggested a model for analyses. Guo and Yao (2021) presented an extensive parametric study about the buckling behavior of perforated plates with rectangular and circular hole shapes. Evaluated plates have been considered as simply supported and investigated with different parameters in their study. Kim et al. (2021) were investigated the perforated plates subjected to uni axial compression loadings by using the commercial finite element analysis program and experimentally. They were considered thickness, aspect ratio and opening size as variables in their study. Silveira et al. (2021) were studied about perforated plate buckling which has elliptical-shaped holes. They

numerically simulated the models with software using the Finite Element Method and square steel perforated plates have a symmetric geometry. Plates were simply supported in its four edges and submitted to a biaxial compressive load and has a centered elliptical cutout. They apply the constructal design method for numerical analysis of the perforated plates. Fu and Wang (2022) were investigated the buckling of perforated plates and for this purpose, they developed a new semi-analytical model by using the Timoshenko shear beam theory in their study and they compare the results with finite element method solutions.

The main objective of this study is to investigate the critical buckling loads of simply supported perforated plates with different perforations and different slenderness ratios under in-plane uniaxial compressive loads numerically. Investigated plates have the same opening sizes with different hole shapes; circular, and square shaped.

2. Material and Methods

Plates can be unstable because of the critical in-plane forces acting on the plates and these forces have effects also on flexural behavior. And also, these plates acting with these forces may undergo buckling by becoming unstable. In engineering practice design for stability is critical. If the in-plane load acting on the square plate is below the critical value and too small to cause buckling, the state of equilibrium is stable. But if the in-plane load is greater than the critical value, the state of

equilibrium is unstable, and this leads to larger deflections.

The general deflection expression which satisfies the boundary conditions of a simply supported rectangular plate can be expressed as an infinite series of as follows:

$$w = \sum_{m=1,2,\dots}^{\infty} \sum_{n=1,2,\dots}^{\infty} a_{mn} \sin \frac{m\pi x}{a} \sin \frac{n\pi y}{b} \quad (1)$$

$$w = \frac{4P}{ab\pi^4 D} \sum_{m=1,2,3,\dots}^{\infty} \sum_{n=1,2,3,\dots}^{\infty} \frac{\sin \frac{m\pi \zeta}{a} \sin \frac{n\pi \eta}{b}}{\left(\frac{m^2}{a^2} + \frac{n^2}{b^2}\right) \frac{m^2 \sigma_{cr} h}{\pi^2 a^2 D}} \sin \frac{m\pi x}{a} \sin \frac{n\pi y}{b} \quad (2)$$

In equation (2) D is the plate flexural rigidity, a is the length of the plate in x axis, b is the length of the plate in y axis, and σ_{cr} is the critical stress value.

When the denominator of one of the terms in equation (2) becomes equal to zero the critical stress value σ_{cr} occurs. This critical value will occur when $n=1$ in equation (2). Equation (3) and Equation (4) give these critical stress values.

In equation (1) w defines the deflection value. This general expression can be customized for a simply supported rectangular plate uniformly lateral loaded in the x direction and carrying a concentrated load P at a point with coordinates ζ and η is as follows.

$$\sigma_{cr} = \frac{\pi^2 a^2 D}{hm^2} \left(\frac{m^2}{a^2} + \frac{1}{b^2}\right)^2 \quad (3)$$

$$\sigma_{cr} = \frac{\pi^2 D}{hb^2} \left(\frac{mb}{a} + \frac{a}{mb}\right)^2 \quad (4)$$

Geometry of a plate model subjected to uniaxial compressive forces is shown in Figure 1.

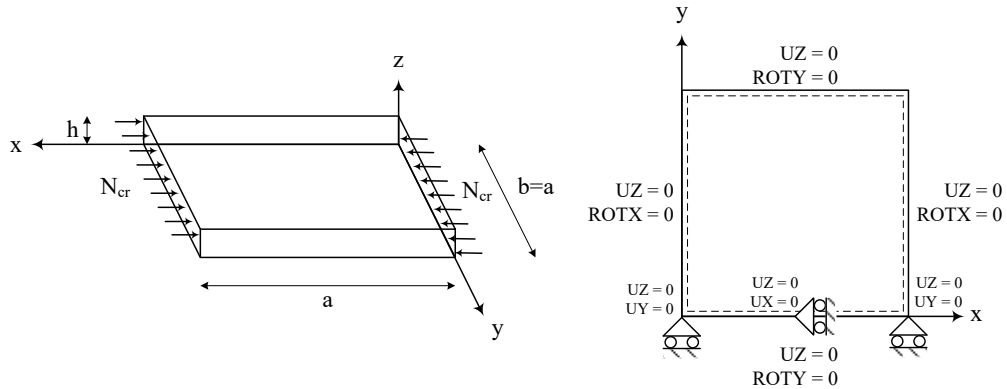


Figure 1. Non-perforated plate model and boundary conditions under uniaxial compressive forces

The elastic critical stress of a square plates subjected to uniform axial compressive stress which are simply

supported along all edges is as follows (Bryan, 1891; Guo & Yao, 2021):

$$\sigma_{cr} = k \frac{\pi^2 E}{12(1-\nu^2)(a/h)^2} \quad (5)$$

In equation (5) E is the elastic modulus, ν is the Poisson's ratio, a is the plate width and h is the plate thickness. Plate buckling coefficient is expressed in equation (5) as k. If D is the plate flexural rigidity (Timoshenko & Woinowsky-Krieger, 1959), plate buckling coefficient is explained in equation (6) and equation (7).

$$k = \sigma_{cr} \frac{ha^2}{D\pi^2} \quad (6)$$

$$D = \frac{Eh^3}{12(1-\nu^2)} \quad (7)$$

The calculation results of the examples discussed in this study were obtained using the ANSYS finite element package program. The 4-node structural shell element SHELL 181 from the ANSYS element library, shown in Figure 2, is used as the finite element. The SHELL 181 element is 4-node structural shell element with different options such as triangular option, membrane option or layered option. Each of the 4 nodes of this element has six degrees of freedom: translations in the x, y, and z directions and rotations in the x, y, and z axes.

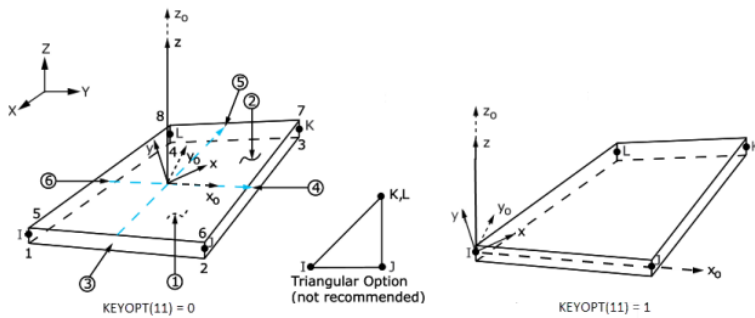


Figure 2. Geometry of SHELL181 finite element in ANSYS (Swanson Analysis System Inc., 2005)

It supports properties such as linear, large rotation, and large strain nonlinear applications (Swanson Analysis System Inc., 2005).

3.Examples

In order to investigate the hole shape effect on buckling of uniaxially loaded square plates, one dimension of the plate is taken as 300 mm, and analyses were performed for non-perforated, square perforated, and circle perforated square plates. Investigated two plates have different hole shapes with the same

opening sizes. Holes on the plates are circular, and square shaped.

Geometry and boundary conditions of the plate model with a circular hole is shown in Figure 3. In the present study, plates are considered to be simply supported on all edges. Freedom of the translational displacement in the plane of the plate and condition of nonoccurrence of rigid body movement should be applied to the models. For this purpose, two joints at the bottom corners were fixed in the y direction and middle joint at the bottom edge was fixed in the x direction.

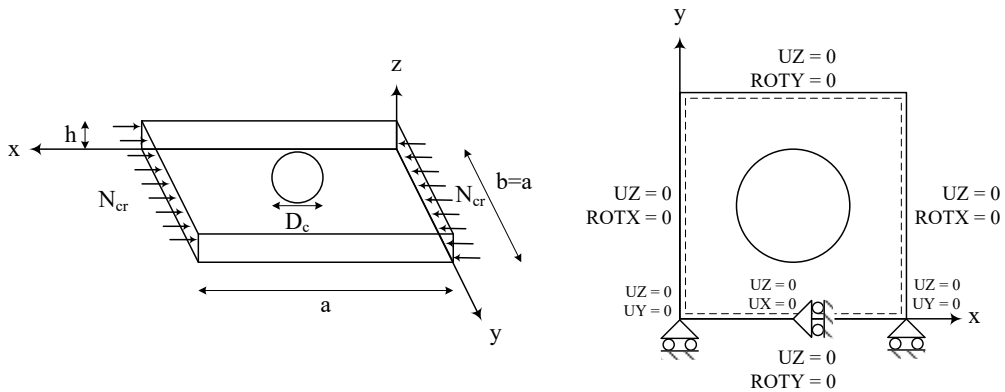


Figure 3. Plate model with a circular hole and boundary conditions.

Dimensions and the loading of the plate is shown in Figure 1 and Figure 3. Material properties of the example plates were modulus of elasticity (E) and Poisson's ratio (ν) are 200000 MPa, and 0.3, respectively.

3.1 Verification of Mesh Quality

The results obtained in numerical simulations performed by the finite element method are dependent on the mesh quality. Results obtained with a poor mesh structure will also give poor or inaccurate results. Therefore, it is necessary to make sure that the mesh is good enough to obtain reliable results. In general, the finer mesh means the more accurately results. But in this case, there are more data points, and the number of nodes and unknowns will increase. To determine the dependence of the results on the mesh quality a mesh independence study is performed.

In this mesh quality study, buckling analyses were performed on a simply supported square steel plate with the dimension 300 mm x 300 mm and a

thickness of 2 mm. A series of models were generated for this sample plate by meshing with finite elements whose size was varying from 50 mm (coarsest mesh) to 2 mm (finest mesh) divisions for mesh quality verification. Critical buckling load yielded from each model were calculated and compared to study the influence of mesh quality on the buckling analysis results. This series of buckling analysis results, comparisons and percentage approximate errors were calculated by comparing other results to the exact results (Timoshenko & Woinowsky-Krieger, 1959) and shown in Figure 4. It can be observed from Figure 4 that when the number of mesh elements along plate length is higher than 60, the increase of mesh density does not significantly improve the accuracy of critical buckling load anymore.

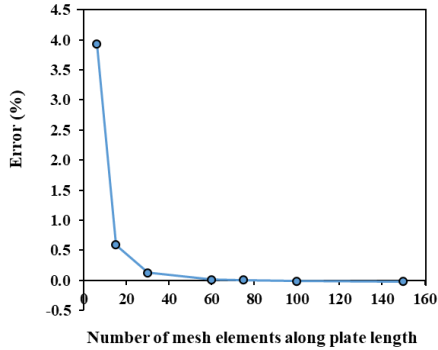


Figure 4. Number of mesh elements vs accuracy for critical buckling load

Different results are obtained with different finite element frequencies created for the analyzed plate models. Because the mesh created for the problems in the finite element method directly affects the results. As the number of elements increases, more accurate results are approached. The frequency of elements more than necessary will cause different numerical errors. In order to determine the correct finite element mesh density, the relationship between element size and critical buckling load is examined by increasing the number of finite elements, and the element size with the same amount of critical buckling load can be determined. As a result of such convergence processes, the finite element size is taken as 5 mm in the problems solved in this study.

3.2 Verification of Finite Element Analysis Models

The correct calculation of the analysis results is directly dependent on the selected element type as well as the finite element mesh density. To evaluate the accuracy of finite element solutions, the obtained results should be compared with experimental results or theoretical values. In this study, in order to verify the finite element solutions, the problems taken from the reference samples were also solved and the convergence of the obtained values was checked.

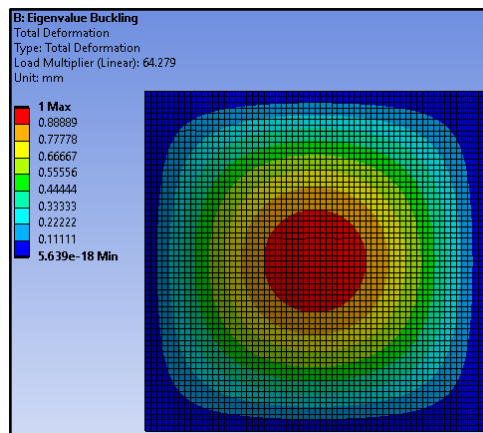


Figure 5. Contour plot of total deformations for a non-perforated plate.

Before investigating the buckling behavior of the perforated plates by using finite element software buckling analyses of the non-perforated plates taken from the literature were performed by using the program to verify the accuracy. For this purpose, the results obtained by finite element method are compared to those results obtained by using an exact solution procedure based on the infinite power series (Timoshenko & Woinowsky-Krieger, 1959). As an example, buckling

analysis was performed for non-perforated square plate by taking the finite element size as 5mm and the contour plot of total deformations of the plate is shown in Figure 5.

Buckling analyses of the other example problems also performed by using the finite-element software and critical buckling loads were obtained.

The buckling coefficient is calculated as in Equation (8).

$$N_{cr} = k \frac{D\pi^2}{b^2} \tag{8}$$

In equation (8) N_{cr} is the critical buckling load. The buckling coefficients obtained by the finite element for the simply supported square plates without holes with different thickness and the corresponding values obtained from Timoshenko and Woinowsky-Krieger (Timoshenko & Woinowsky-Krieger, 1959) are listed in Table 1. Length of square steel plate is taken as 300 mm.

Table 1. Comparison of critical buckling load and buckling coefficients of non-perforated plate

a/h	N_{cr}^{FE} (N/mm)	k^{FE}	$N_{cr}^{(Tim.\&Woi.)}$ (N/mm)	$k^{(Tim.\&Woi.)}$	$k^{Difference\%}$	$N_{cr}^{Difference\%}$
150	64.2790	4.0005	64.2709	4.0000	0.013	0.013
100	216.8800	3.9994	216.9144	4.0000	-0.016	-0.016
50	1732.1000	3.9926	1735.3151	4.0000	-0.185	-0.185

Difference% values are calculated by the formula in equation (9):

$$Difference\% = \frac{FE-Reference}{Reference} \times 100 \tag{9}$$

It can be seen from the Table1 that there is a good consistency of the buckling coefficients and loads obtained from finite element method and numerical results from literature. These results

indicate that the finite element method models presented in this paper is reliable and accurate. And also, critical buckling load for simply supported square plate with a circular hole is verified from El-Sawy and Nazmy (El-Sawy & Nazmy, 2001) and shown in Table 2. In the middle of the square plate, a circular hole is perforated, and the diameter was taken as 150mm which is half of the square plate length.

Table 2. Comparison of critical buckling load and buckling coefficients of a square plate with a circular hole

a/h	N_{cr}^{FE} (N/mm)	k^{FE}	$N_{cr}^{(El.\&Naz.)}$ (N/mm)	$k^{(El.\&Naz.)}$	$k^{Difference\%}$	$N_{cr}^{Difference\%}$
150	46.6390	2.9026	46.5964	2.9000	0.091	0.091
100	157.2800	2.9003	157.2629	2.9000	0.011	0.011
50	1253.9000	2.8903	1258.1034	2.9000	-0.334	-0.334

3.3 Finite Element Analysis Models

Analyses were performed for square plates with a square, and circular hole of different open area ratios and different slenderness ratios ($a/h = 50, 100,$ and 150). Plate surface areas are constant as

300 mm x 300 mm. Square plates with circular holes were taken as reference and the open area in each problem was modeled equally so that the sample problems could be compared with each other.

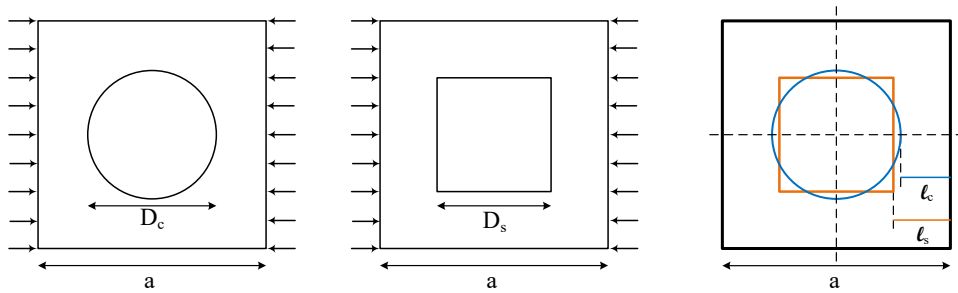


Figure 6. Plane view of square plate models with circle and square hole shapes.

A schematic plan view for one of the example problems which has the same open area is shown in Figure 6. The notation l_s is the length between the line of action of the load and the square hole edge in the middle of the plate and the notation l_c is the similar length for the circle hole.

Boundary conditions are simply supported in four edges as shown in Figure 1. A uniform unit load is applied to the edges of $x=0$ and $x=a=300\text{mm}$ and performed the eigenvalue analysis by using the finite element software program. After obtaining the lowest eigenvalue, the critical buckling load N_{cr} was calculated. The effect of slenderness ratio, open area ratio, and hole shape on the critical buckling load of perforated square plates loaded with uniaxial compression are presented in Table 3. In the analyses, both cases of rectangular and circular holes in the middle of the plates are considered.

The variation of the length l_s is for square perforated plate and the length l_c for circle perforated plate versus the hole area is shown in Figure 7.

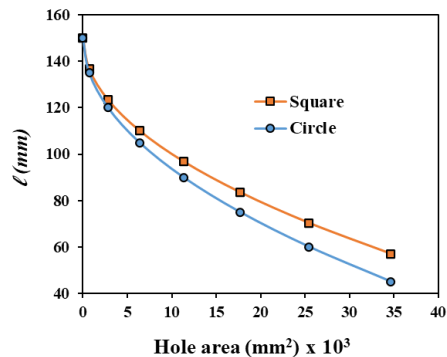


Figure 7. Variation of the location of the edge lines of the circular and square holes.

Figure 8 compares the critical buckling loads for simply supported square plates with square and circular holes. In this figure slenderness ratios of the plates are 150 so that 300 x 300 dimensioned plate thickness is 2 mm.

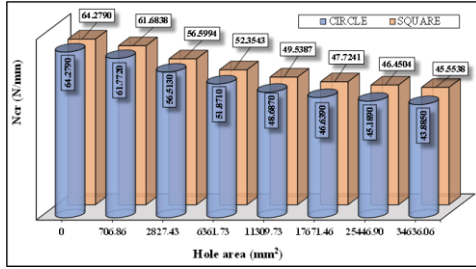


Figure 8. Critical buckling loads for perforated square plates (a/h=150).

In Figure 9 and Figure 10, the buckled shapes of the example plates are shown, indicating the formation of only one half-wave for all hole diameters used. In these seven example problems, the hole areas of the square holes are the same as the circle holes.

Table 3 Comparison of critical buckling loads with different parameters

Model no	h (mm)	Hole area (mm ²)	Open area ratio (%)	D _c (mm)	ℓ _c (mm)	N _{cr} (N/mm)	D _s (mm)	ℓ _s (mm)	N _{crs} (N/mm)
1	2	0.00	0.00	0	150	64.279	0.000	150.000	64.279
2	2	706.86	0.79	30	135	61.772	26.587	136.707	61.684
3	2	2827.43	3.14	60	120	56.513	53.174	123.413	56.599
4	2	6361.73	7.07	90	105	51.871	79.760	110.120	52.354
5	2	11309.73	12.57	120	90	48.687	106.347	96.826	49.539
6	2	17671.46	19.63	150	75	46.639	132.934	83.533	47.724
7	2	25446.90	28.27	180	60	45.189	159.521	70.240	46.450
8	2	34636.06	38.48	210	45	43.885	186.108	56.946	45.554
9	3	0.00	0.00	0	150	216.880	0.000	150.000	216.880
10	3	706.86	0.79	30	135	208.420	26.587	136.707	208.076
11	3	2827.43	3.14	60	120	190.680	53.174	123.413	190.882
12	3	6361.73	7.07	90	105	175.010	79.760	110.120	176.523
13	3	11309.73	12.57	120	90	164.240	106.347	96.826	166.967
14	3	17671.46	19.63	150	75	157.280	132.934	83.533	160.754
15	3	25446.90	28.27	180	60	152.300	159.521	70.240	156.329
16	3	34636.06	38.48	210	45	147.730	186.108	56.946	153.138
17	6	0.00	0.00	0	150	1732.100	0.000	150.000	1732.100
18	6	706.86	0.79	30	135	1664.600	26.587	136.707	1660.760
19	6	2827.43	3.14	60	120	1523.100	53.174	123.413	1522.322
20	6	6361.73	7.07	90	105	1397.900	79.760	110.120	1406.602
21	6	11309.73	12.57	120	90	1311.100	106.347	96.826	1328.598
22	6	17671.46	19.63	150	75	1253.900	132.934	83.533	1276.296
23	6	25446.90	28.27	180	60	1211.300	159.521	70.240	1237.184
24	6	34636.06	38.48	210	45	1169.600	186.108	56.946	1206.876

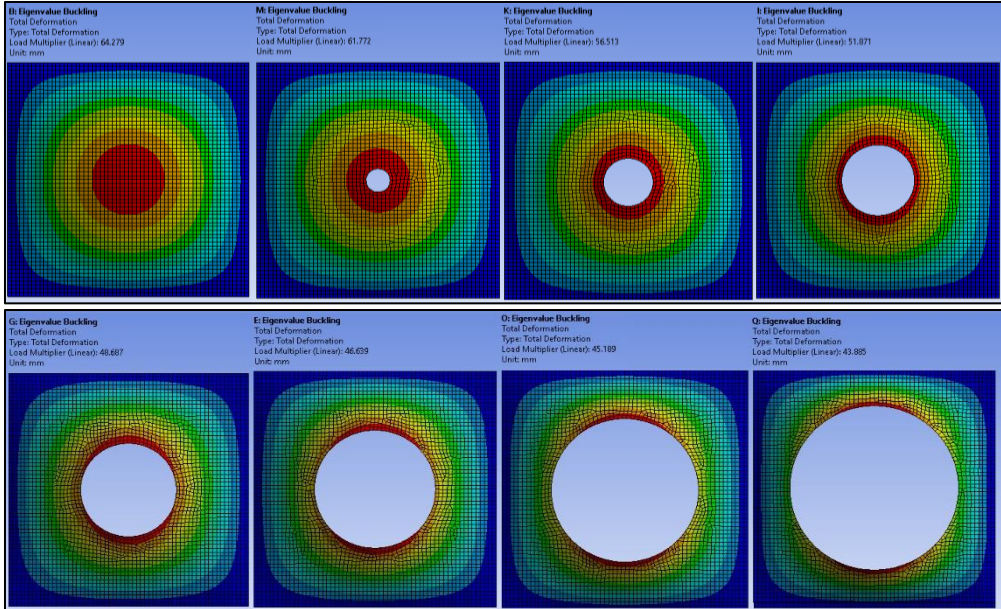


Figure 9. Buckling mode shapes for circle plate models with different hole areas.

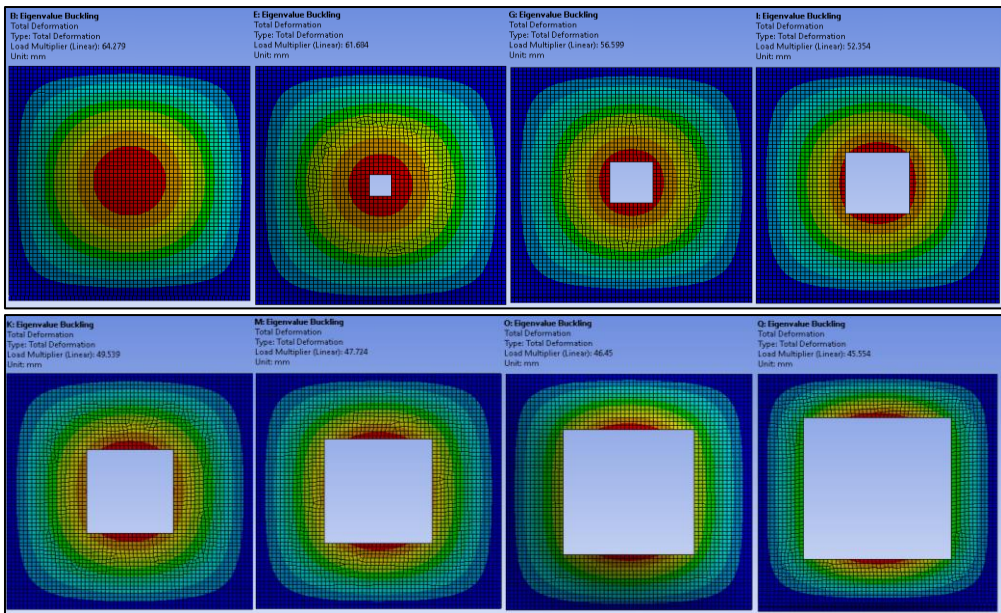


Figure 10. Buckling mode shapes for square plate models with different hole areas.

4.Results and Discussion

The critical buckling loads of simply supported different hole shaped perforated plates subjected to in-plane

uniaxial compressive loads have been investigated numerically. Analyses were performed by using commercial finite element software package ANSYS. As a result of these simulations, it is observed

that when the hole area increases the critical buckling loads also decrease as expected. Because the plate rigidity was also decreased by the perforation.

In order to compare the results more accurately, the hole areas of the square-hole plates and the circular-hole plates were taken as the same. It is interesting that critical buckling loads of circular perforated plates are lower than the square perforated plates with the same hole area. Similar to what Brown et al. mentioned in their study (Brown et al., 1987), if the length between the line of action of the load and the hole edge in the middle of the plate is longer, this eventually increases the critical buckling load with the increased area between the edge of the square plate and the hole. Thus, the critical buckling load of a square hole plate is greater than for a circle hole plate which has the same boundary conditions and loadings.

As shown in Figure 7, the length l_s is greater than the length l_c for all considered example problems. As the hole area increases, the difference between the defined lengths increases, and accordingly the critical buckling loads for plates with square holes also increase. This result could be seen in detail in Figure 8 for the a/h ratio of 150. The graphs of critical buckling loads versus open hole areas for thicker plates with slenderness ratios of 100 and 50 are similar to this graph, but only the values of the loads change.

Analyses results of critical buckling loads for simply supported square plates with square and circle holes with the same hole ratio are shown in Figure 9 and Figure 10. It can be seen from the

figures that when the hole area decreases total deformation of the plate increases especially at the edges of the holes. In the last two models whose hole area is larger, this value is more dominant at the edge of the hole perpendicular to the lines where uniaxial buckling loads are applied.

5. Conclusion

The critical buckling loads prediction of staggered arranged perforated plates with holes of different geometries stainless steel plates under compressive loading was investigated by finite element analysis software. For this purpose, buckling analyses of perforated plates with different hole shapes of perforation and slenderness ratios were carried out. Centrally located circular and square holes in square plates subjected to uniaxial buckling load have been considered and analyzed for simply supported boundary conditions. The following are some conclusions that can be drawn based on the numerical outcomes of the problems:

- Increasing the size of the hole area will reduce the critical buckling load of simply supported perforated rectangular plates aforementioned in this study.
- As the hole area increases, the length between the action line of the uniaxial load and the circle hole edge in the middle of the plate decreases more than the length between the square hole edge.
- The critical buckling load of square and circular hole simply supported square plates with the same

hole area loaded with uniaxial buckling load is higher for plates with square holes than for plates with circular holes.

6. References

- Albayrak, U., & Saraçoğlu, M. H. (2018). Analysis of Regular Perforated Metal Ceiling Tiles. *International Journal of Engineering and Technology*, 10(6), 440–446. doi: 10.7763/ijet.2018.v10.1099
- Bader Al-Amar Mohammed S Hassan AL-Araji, Q. H. (2017). Buckling of Perforated and Unperforated Stiffened Plate. In *Journal of Babylon University/Engineering Sciences*.
- Brown, C J. (1990). Elastic buckling of perforated plates subjected to concentrated loads. *Computers and Structures*, 36(6), 1103–1109.
- Brown, Christopher J, Yettram, A. L., & Burnett, M. (1987). Stability of Plates with Rectangular Holes. *Journal of Structural Engineering*, 113(5), 1111–1116. doi: 10.1061/(ASCE)0733-9445(1987)113:5(1111)
- Bryan, G. H. (1891). On the stability of a plane plate under thrusts in its own plane with applications to the buckling of the sides of a ship. *Proceedings of London Mathematics Society*, 54–67.
- da Silveira, Thiago, Torres Pinto, V., Pedro Sarasol Neufeld, J., Pavlovic, A., Alberto Oliveira Rocha, L., Domingues dos Santos, E., & André Isoldi, L. (2021). Applicability evidence of constructal design in structural engineering: case study of biaxial elasto-plastic buckling of square steel plates with elliptical cutout. *J. Appl. Comput. Mech*, 7(2), 922–934. doi: 10.22055/JACM.2021.35385.2647
- El-Sawy, K. M., & Nazmy, A. S. (2001). Effect of aspect ratio on the elastic buckling of uniaxially loaded plates with eccentric holes. *Thin-Walled Structures*, 39, 983–998. Retrieved from www.elsevier.com/locate/tws
- El-Sawy, K. M., Nazmy, A. S., & Martini, M. I. (2004). Elasto-plastic buckling of perforated plates under uniaxial compression. *Thin-Walled Structures*, 42(8), 1083–1101. doi: 10.1016/J.TWS.2004.03.002
- Fu, W., & Wang, B. (2022). A semi-analytical model on the critical buckling load of perforated plates with opposite free edges. *Original Research Article Proc IMechE Part C: J Mechanical Engineering Science*, 236(9), 4885–4894. doi: 10.1177/09544062211056890
- Guo, Y., & Yao, X. (2021). Buckling Behavior and Effective Width Design Method for Thin Plates with Holes under Stress Gradient. doi: 10.1155/2021/5550749
- Karakaya, C. (2022). Numerical investigation on perforated sheet metals under tension loading. *Open Chemistry*, 20(1), 244–253. doi: 10.1515/chem-2022-0142
- Kim, J. H., Park, D. H., Kim, S. K., Kim, J. D., & Lee, J. M. (2021). Lateral deflection behavior of perforated steel plates: Experimental and numerical approaches. *Journal of Marine Science and Engineering*, 9(5). doi: 10.3390/jmse9050498
- Komur, M. A. (2011). Elasto-plastic buckling analysis for perforated steel plates subject to uniform compression. *Mechanics Research Communications*, 38(2), 117–122. doi: 10.1016/J.MECHRESCOM.2011.01.001
- Komur, M. A., & Sonmez, M. (2008). Elastic buckling of perforated plates subjected to linearly varying in-plane loading. *Structural Engineering and Mechanics*, 28(3), 353–356. doi: 10.12989/SEM.2008.28.3.353
- Maiorana, E., Pellegrino, C., & Modena, C. (2008). Linear buckling analysis of perforated plates subjected to localised symmetrical load. *Engineering Structures*, 30(11), 3151–3158. doi: 10.1016/J.ENGSTRUCT.2008.04.024
- Maiorana, E., Pellegrino, C., & Modena, C. (2009). Non-linear analysis of perforated

- steel plates subjected to localised symmetrical load. *Journal of Constructional Steel Research*, 65(4), 959–964. doi: 10.1016/J.JCSR.2008.03.018
- Narayanan, R., & der Avanessian, N. G. V. (1984). Elastic buckling of perforated plates under shear. *Thin-Walled Structures*, 2(1), 51–73. doi: 10.1016/0263-8231(84)90015-6
- Rezaeepazhand, J., & Sabori, H. (2008). Buckling of perforated plates repaired with composite patches. *Key Engineering Materials*, 385–387, 377–380. Trans Tech Publications Ltd. doi: 10.4028/www.scientific.net/kem.385-387.377
- Saraçoğlu, M. H., & Albayrak, U. (2016). Linear static analysis of perforated plates with round and staggered holes under their self-weights. *Research on Engineering Structures & Materials*, 2(1), 39–47. doi: 10.17515/resm2015.25me0910
- Saraçoğlu, M. H., Uslu, F., & Albayrak, U. (2020). Stress and displacement analysis of perforated circular plates. *Challenge Journal of Structural Mechanics*, 6(3), 150. doi: 10.20528/cjsmec.2020.03.006
- Saraçoğlu, M., Uslu, H., & Albayrak, F. (2021). Investigation of Hole Shape Effect on Static Analysis of Perforated Plates with Staggered Holes. *International Journal of Engineering and Innovative Research*, 3(2), 133–144. doi: 10.47933/ijeir.883510
- Seifi, R., Chahardoli, S., & Akhavan Attar, A. (2017). Axial buckling of perforated plates reinforced with strips and middle tubes. *Mechanics Research Communications*, 85, 21–32. doi: 10.1016/J.MECHRESCOM.2017.07.015
- Shakerley, T. M., & Brown, C. J. (1996). Elastic buckling of plates with eccentrically positioned rectangular perforations. *International Journal of Mechanical Sciences*, 38(8–9), 825–838. doi: 10.1016/0020-7403(95)00107-7
- Shanmugam, N. E., Thevendran, V., & Tan, Y. H. (1999). Design formula for axially compressed perforated plates. *Thin-Walled Structures*, 34(1), 1–20. doi: 10.1016/S0263-8231(98)00052-4
- Silveira, T., Neufeld, J. P. S., Rocha, L. A. O., Santos, E. D., & Isoldi, L. A. (2021). Numerical analysis of biaxial elastoplastic buckling of perforated rectangular steel plates applying the Constructal Design method. *IOP Conf. Ser.: Mater. Sci. Eng.* doi: 10.1088/1757-899X/1048/1/012017
- Soares Junior, R.A., Palermo Junior, L., & Wrobel, L.C. (2019). Buckling of perforated plates using the dual reciprocity boundary element method. In *Boundary Elements and other Mesh Reduction Methods XLII* (Vol. 126, pp. 89–100). WIT Press. doi: 10.2495/BE420081
- Soleimani, S., Davar, A., Jam, J. E., Zamani, M. R., & Beni, M. H. (2020). Thermal buckling and thermal induced free vibration analysis of perforated composite plates: a mathematical model. *Mechanics of Advanced Composite Structures*, 7, 15–23. doi: 10.22075/mac.2019.16556.1181
- Swanson Analysis System Inc., A. (2005). *ANSYS User's manual*.
- Timoshenko, S., Woinowsky-Krieger, S. (1959). *Theory of Plates and Shells*. In McGraw-Hill, Inc. McGraw-Hill, Inc.
- Yanli, G., Xiaoqing, S., Xiao, L., Xingyou, Y., Zhifan, X., Bin, X., Jianyi, S. (2019). Elastic buckling of thin plate with circular holes in bending. *E3S Web of Conferences*, 136, 3–8. doi: 10.1051/e3sconf/201913604043

Araştırma Makalesi / Research Article

**Evaluation of the Combined Effects of Long-Term Aging
And Moisture Damage on the Performance of Asphalt
Mixture Incorporating Warm Mix Additive**

*¹Teh Sek Yee, ²Tan Shin Ru, ³Meor Othman Hamzah, ⁴Seyed Reza Omranian,
⁵Mohd Rosli Hainin

¹Edgenta Infrastructure Services, Bangsar South, 59200 Kuala Lumpur, Wilayah Persekutuan Kuala Lumpur, Malaysia, erictch@edgenta.com, ORCID ID: <http://orcid.org/0000-0002-6558-1358>

²Green Enable Technologies Sdn. Bhd., Lot 2764, Mukim Kampung Buaia, 33700 Padang Rengas, Perak, Malaysia, shinrutan@ytlcement.com.my, ORCID ID: <http://orcid.org/0000-0002-0988-6907>

³School of Civil Engineering, Universiti Sains Malaysia, 14300 Nibong Tebal, Pulau Pinang, Malaysia, meorothmanhamzah@gmail.com, ORCID ID: <http://orcid.org/0000-0002-5195-8257>

⁴Faculty of Applied Engineering, EMIB-Research Group, University of Antwerp, 171 Groenenborgerlaan, Antwerp 2020, Belgium, seyedreza.omranian@uantwerpen.be, ORCID ID: <http://orcid.org/0000-0001-6677-3784>

⁵College of Engineering, Universiti Malaysia Pahang, 26600 Pekan, Pahang, Malaysia, roslihainin@ump.edu.my, ORCID ID: <http://orcid.org/0000-0001-8494-7055>

Geliş / Received: 30.10.2022;

Kabul / Accepted: 31.12.2022

Abstract

Infiltration of moisture into the Warm Mix Asphalt (WMA) mixture is one of the primary factors that potentially compromises pavement structural integrity. This paper evaluates the effectiveness of a warm mix additive as an antistripping agent in WMA. In this study, to simulate field environmental conditions in the laboratory, asphalt mixture specimens were first exposed to long-term aging and moisture damage (simultaneously). Different aspects of WMA and Hot Mix Asphalt (HMA) performance including compactability, workability, tensile and shear strengths were then studied and compared. A 3D image analysis was performed to precisely quantify the percentage of failure contributed by adhesion on the fractured surface of the tested specimens. The test results showed that WMA samples were not only more workable and compactable compared to HMA but also exhibited superior resistance toward

*¹Sorumlu yazar / Corresponding author

Bu makaleye atıf yapmak için

Yee, T.S., Ru, T.S., Hamzah, M.O., Omranian, S.R. & Hainin M.R.M. (2022). Evaluation of the Combined Effects of Long-Term Aging And Moisture Damage on the Performance of Asphalt Mixture Incorporating Warm Mix Additive. *Journal of Innovations in Civil Engineering and Technology (JICIVILTECH)*, 4(2), 77-95.

moisture damage over HMA even after experiencing severe moisture conditioning. Such trend was also observed based on higher strength and lower adhesion failure of WMA compared to HMA, regardless of test type. The tensile and shear stresses results indicated that utilization of cubical aggregates in asphalt mixtures can improve mixture performance. Moreover, the 3D image analysis results showed that the cubical aggregates utilized to prepare modified WMA exhibited lower adhesion failure which could be correlated to the effectiveness of the WMA additive.

Keywords: *Warm mix additive, Cubical aggregates, Moisture conditioning, Long-term aging, Imaging technique.*

Ilık Karışım Katkısı Katılan Asfalt Karışımının Performansına Uzun Süreli Yaşlanma ve Nem Zararının Birleştirilmiş Etkilerinin Değerlendirilmesi

Öz

Ilık Karışım Asfalt (WMA) karışımına nemin sızması, kaplamanın yapısal bütünlüğünü potansiyel olarak tehlikeye atan birincil faktörlerden biridir. Bu makale, ılık karışım katkı maddesinin WMA'da soyulma önleyici bir madde olarak etkinliğini değerlendirmektedir. Bu çalışmada, laboratuvarında saha ortam koşullarını simüle etmek için, asfalt karışım numuneleri önce uzun süreli yaşlanma ve nem hasarına (eşzamanlı olarak) maruz bırakılmıştır. Daha sonra sıkıştırılabilirlik, işlenebilirlik, çekme ve kesme dayanımları dahil olmak üzere WMA ve Sıcak Karışım Asfalt (HMA) performansının farklı yönleri incelendi ve karşılaştırıldı. Test edilen numunelerin kırık yüzeyindeki yapışmanın neden olduğu bozulma yüzdesini kesin olarak ölçmek için bir 3D görüntü analizi yapıldı. Test sonuçları, WMA numunelerinin HMA'ya kıyasla yalnızca daha fazla işlenebilir ve sıkıştırılabilir olduğunu değil, aynı zamanda şiddetli nem koşullandırmasına maruz kaldıktan sonra bile HMA'ya göre nem hasarına karşı üstün direnç sergilediğini gösterdi. Bu eğilim, test türünden bağımsız olarak, HMA'ya kıyasla WMA'nın daha yüksek mukavemeti ve daha düşük yapışma bozulmasına dayalı olarak da gözlemlendi. Çekme ve kayma gerilmeleri sonuçları, asfalt karışımlarda kübik agrega kullanımının karışım performansını iyileştirebileceğini göstermiştir. Ayrıca, 3D görüntü analizi sonuçları, modifiye WMA'yı hazırlamak için kullanılan kübik agregaların, WMA katkı maddesinin etkinliği ile ilişkilendirilebilecek daha düşük yapışma bozulması sergilediğini gösterdi.

Anahtar kelimeler: *Ilık karışım katkı maddesi, Kübik agregalar, Nem şartlandırması, Uzun süreli yaşlandırma, Görüntüleme tekniği.*

1. Introduction

Warm Mix Asphalt (WMA) has recently gained popularity among road construction industries due to their lower mixing and compaction temperatures compared to Hot Mix Asphalt (HMA) (Barraj, F., et al., 2022). This results in reduction of greenhouse gas emissions and energy consumption. Despite the beneficial impacts, WMAs are susceptible to moisture damage as ramification of lower mixing and compaction temperatures leading to incomplete drying, hence the presence of trapped moisture within the aggregate particles. According to Hicks (1991), the two main mechanisms associated with moisture damage are adhesion failure due to presence of water at the interface between mixture constituents which facilitate the removal of binder film from the aggregate surface, and of cohesion failure due to the changes in asphalt mastics or mortar softening point in the presence of moisture. Copeland et al. (2007) later on recognized aggregate degradation as the third mechanism in which moisture degrades the bituminous mixtures. Wen et al. (2016) suggested that the addition of an antistripping agent in WMA can considerably improve the stripping inflection point due to moisture damage. One of the recently developed WMA additives is ZycoTherm. This additive can reduce the mixture compaction temperatures to approximately 110°C. Rohith and Ranjitha (2013) reported compatibility of ZycoTherm with both unmodified and modified binders due to its insignificant influence on the binder properties and grade. Sharanappanavar (2013) also found lower mixing and

compaction temperatures of WMA mixtures modified using ZycoTherm, It was also stated that such additives can potentially act as an anti-stripping agent to enhance the moisture resistance of asphaltic mixtures.

In reality, asphalt pavements are subjected to several distresses such as moisture damage and long-term aging. The aging increases the mixture stiffness and brittleness, particularly at low temperatures (Hamzah et al., 2015). Similarly Menapace et al. (2015) informed that although aging exhibited negligible impacts on the microstructure morphology of WMA binders, such effects could considerably influence the asphalt mechanical properties. Bairgi et al. (2018) found the beneficial impacts of densification and long-term field aging on WMA rutting and stripping characteristics. According to Izadi et al. (2018), although aging increased the fracture energy and failure resistance of both WMA and HMA, long-term aging significantly reduced the mixtures' fatigue life. However, the detrimental effects of aging on the mechanical properties of WMA were found to be lower compared to the corresponding values of HMA. Arefin et al. (2018) found that binder type plays a crucial role on the effects of aging on both WMA and HMA. Valentová et al. (2016) reported the effects of aging on mixtures' moisture susceptibility in terms of Indirect Tensile Strength Ratio (ITSR), containing either only regular paving grade bitumen or bituminous binder with combination of anti-stripping agents or WMA additives. From their

study, the additive initially showed reduced ITR after 5 days of laboratory aging, but improved ratio after 9 days of aging.

The objectives of this study are: to first assess the moisture susceptibility of mixtures incorporating warm mix additive under different circumstances such as simultaneous long-term aging and moisture damage; to measure the proportions of adhesive failure and broken aggregates via 3D imaging technique, and finally to evaluate and compare the compactibility and performance of specimens when normal and cubical aggregates were used to prepare asphalt mixtures. Two types of asphaltic mixtures subjected to various conditions including, unconditioned and simultaneous three freeze-thaw (3 F-T) cycles and long-term aging (LTA) were prepared. The additive was incorporated as the anti-stripping and warm compaction additive in WMA to investigate the effects of lower compaction temperature on the mixtures' moisture damage susceptibility. The performance of asphalt mixtures in terms of tensile and shear strengths was also evaluated.

2 Materials and Methods

2.1 Materials

WMA samples incorporating the warm mix additive with 80/100 penetration grade (PG-64) base binder, normal and geometrically cubical shaped granite

aggregates were first prepared in accordance with local specifications for asphalt mixture type AC 14 (JKR 2008). HMA mixtures were also prepared to serve as control samples. Tables 1 to 3 provides the basic properties of raw materials and aggregate gradation. Ordinary Portland Cement (OPC) was the filler type used. As a continuation from a previous study conducted by Kuan (2017), 5.3% optimum binder content was adopted in the preparation of all specimens. To prepare the modified binder, the base binder and high shear mixer mould utilized for wet mixing were preheated at 140°C in an oven for two hours prior to blending. A warm mix additive, 0.1% by binder mass, was then added to the base binder and premixed homogenously at 1,000 rpm for 10 minutes. The properties of the added additive are tabulated in Table 4. From the Rotational Viscometer test results, the mixing and compaction temperatures for HMA were determined as 160°C and 150°C, respectively, while the corresponding values were reduced to 140°C and 130°C for the preparation of WMA. Prior to the mixing procedures, the batched aggregates were preheated in an oven for four hours at the target compaction temperature, while the base and modified binders were only preheated for two hours at the same temperature to minimise premature aging of binder. The loose mixtures were finally compacted to 7±1% air voids using a gyratory compactor.

Table 1. Granite aggregate properties.

Feature	Measured Values
Specific Gravity (g/cm ³)	2,62
Water Absorption Ratio (%)	0,91
Los Angeles Abrasion Loss Value (%)	23,86
Aggregate Crushing Value (%)	19,25
Coarse Aggregate Angularity (%)	49,51
Flat and Elongated (%)	23,3

Table 2. Binder PG-64 properties.

Feature	Measured Values
Penetration at 25°C, 100 g, 5 s, (0.1 mm)	85,8
Softening Point (°C)	45
Ductility at 25°C (cm)	>100
Flash and Fire Point (°C)	331-340
Solubility (%)	99,52
Specific Gravity (g/cm ³)	1,03

Table 3. Aggregate gradation for mix type AC14 (JKR, 2008)

Sieve Sizes (mm)	20	14	10	5	3,35	1,18	0,425	0,15	0,075
Lower-Upper Limits	100	90-100	76-86	50-62	40-54	18-34	12-24	6-14	4-8
Passing (%)	100	95	81	56	47	26	18	10	6

Table 4. Properties of the warm mix additive

Criteria	Descriptions
Form	Liquid
Color	Pale yellow
Flash Point (°C)	>80
Density (g/ml)	1.01
Freezing Point (°C)	5
Solubility	Miscible in water
pH Value	10% solubility in water neutral or slightly acidic
Viscosity (CPS)	100-500

2.2 Mixtures Conditioning Methods

In addition to unconditioned samples (control), some of the compacted specimens were long-term aged and moisture conditioned to simulate the field conditions. The SHRP-A-383 (Bell et al., 1994) procedures were modified where compacted samples were exposed

to ultraviolet light at 85°C for five days in a forced-draft oven to prepare the long-term aged specimens. To accelerate the adverse effects of field water intrusion in asphalt pavements, the aged specimens were then fully immersed in a vacuum saturator filled with sodium

carbonate solution at 6.62 gm/litre concentration for moisture conditioning following ASTM D4867 (ASTM, 2006) procedures. A saturation level of 55% to 80% was achieved by vacuuming compacted specimens in the desiccator for 15 minutes. The vacuum saturation procedures were repeated when the degree of saturation was less than 55%, while the specimens were considered as damaged and discarded when the

degree of saturation was more than 80%. Specimens were then frozen at $-18 \pm 2^{\circ}\text{C}$ for at least 15 hours, followed by immersion in water bath at 60°C for 24 hours as one cycle. The above procedure was repeated for three cycles. For ease of reference, the mixtures were designated based on their constituents and conditioning methods as exemplified in Table 5.

Table 5. Designation of tested mixtures

Mixture Type	Aggregate Type	Conditioning	Mixtures Designation
Hot Mix Asphalt	Normal	Unconditioned	HNU
		Conditioned	HNC
	Cubical	Unconditioned	HCU
		Conditioned	HCC
Warm Mix Asphalt	Normal	Unconditioned	WNU
		Conditioned	WNC
	Cubical	Unconditioned	WCU
		Conditioned	WCC

2.3 Determination of Compaction Energy and Workability Indices

The Compaction Energy Index (CEI) indicates the consumed energy by the roller during execution in order to compact loose asphalt mixtures to the desired in-situ density. The CEI was obtained from the maximum specific gravity (G_{mm}) values from the 8th gyration to 92% of Gmm. The Gmm value of the 8th gyration was used to mimic the compaction effort by the paver during construction, while the selection of 92% Gmm was based on the current state of practice where HMA mat was initially roller-compacted to 92% Gmm, and subsequently compacted under traffic loading. The CEI equals the area under the curve between the 8th

gyration and 92% Gmm as shown in Figure 1. Although lower CEI is generally desirable, mixtures with very low CEI value might result in a tender pavements which should be avoided (Mahmoud and Bahia, 2004).

Moreover, the mixture workability was calculated based on Leeds Workability Method (Cabrera, 1991). The Leeds method is based on the relationship between mixture air voids and the corresponding compaction energy input applied by the gyratory compactor. A higher Workability Index (WI) indicates mixtures that are easier to compact (Dessouky et al., 2012). It should be

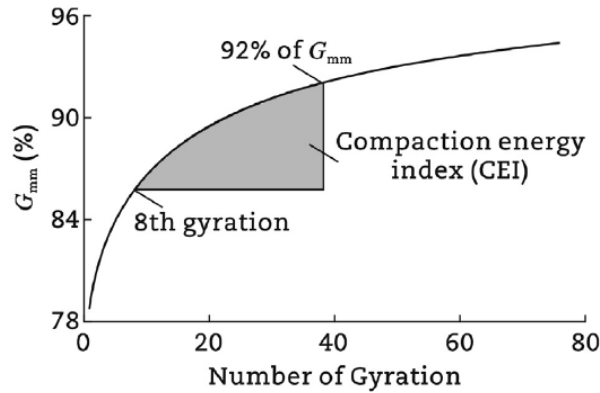


Figure 1. Illustration of the compaction energy index (Mahmoud and Bahia, 2004)

informed that in order to minimizing compaction effort lower CEI and higher WI mixtures are more desirable.

2.4 Leutner Shear Test

The Leutner shear test is typically used to determine the pavement layers bonding condition. In this study, the test was conducted to determine the effects of aggregate shape and warm mix additive on the shear strength of asphalt specimens. In the test, the samples were first pre-conditioned at 10°C in an incubator for four hours prior to testing. The conditioned specimens were placed in the Leutner shear frame with interchangeable clamping and loading devices, and properly aligned with the shear axis as shown schematically in Figure 2. A constant loading rate of 50.8 mm/min was then applied until the specimens were sheared into two parts and the maximum shear force was obtained. Displacement recordings allowed the relationship between shear load versus displacement to be plotted.

The Leutner shear strength was calculated using Equation (1). The Leutner shear strength ratio as an aging index was also computed as the strength ratio of conditioned to unconditioned specimens.

$$\sigma_s = F_{\max}/A \quad (1)$$

where, σ_s is the shear strength (MPa), F_{\max} represents the maximum shear force (kN), A is the specimen cross sectional area (m²).

2.5 Semi-Circular Bending Test

The Semi-Circular Bending (SCB) test is typically used to characterize mixtures' fracture properties (Omranian et al., 2017). The test was carried out in accordance with AASHTO TP 124 (AASHTO, 2016) procedures to measure the tensile strength of asphalt mixtures. Semi-circular specimens with a notch at the center of flat side were first prepared. The specimens were conditioned at 10°C

in an incubator for four hours prior to testing. A SHIMADZU Universal

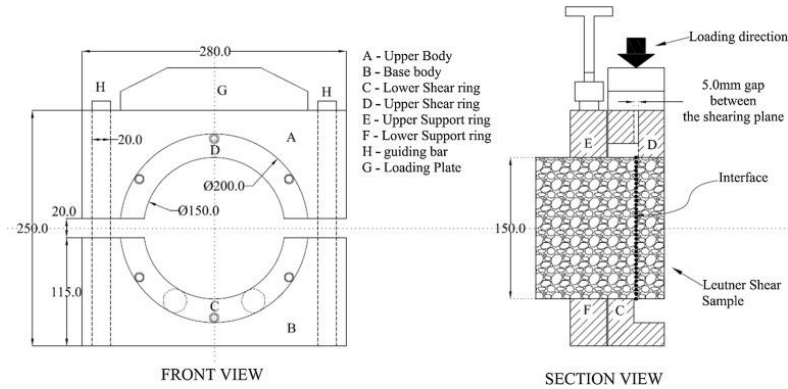


Figure 2. Schematic of leutner shear test (Sudarsanan et al., 2018)

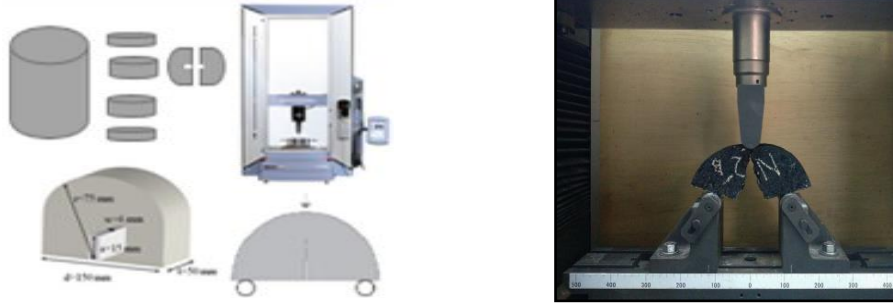
Testing Machine equipped with SCB test setup was employed to perform the test. Two roller supports were set at $120 \pm 0,1$ mm distance apart. A semi-circular specimen was placed on the roller supports and the load cell of 100 kN was aligned with the notch at the centre. The load was then applied at a constant rate of 50.8 mm/min until the specimen split into two. Figure 3 presents a schematic sketch of specimens and their preparation, testing apparatus as well as the split samples. The maximum tensile strength was calculated using Equation 2. The tensile strength ratio was also computed as the strength ratio of conditioned to unconditioned specimens.

$$\sigma_{\max} = 4,253F_{\max}/Dt \quad (2)$$

where, F_{\max} is the maximum force (N), D equals the specimen diameter (mm), and t is the specimen thickness (mm). In total, three replicates for each tested mixture were evaluated.

2.6 Imaging Technique

Upon close visual examination, three distinct colours can be observed on the fractured surfaces of the tested specimens. These colours were related to failures caused by adhesion (brownish), cohesion (black) and broken aggregates (white). A 3D image analysis technique was carried out to measure the percentages of adhesion and cohesion failures as well as broken aggregates due to moisture damage. The 2D images of the fractured surface of the tested samples were initially captured using a high-resolution optical device. At least 20 images at equally spaced intervals



(a) Schematic of Semi-Circular Bending Test (Omranian et al., 2018a) (b) Split Sample

Figure 3. SCB test

were taken for each specimen. Figure 4 shows the schematic image capturing procedures. The conventional 2D photos were converted into a 3D model using the Autodesk ReCap Photo software. The completed 3D models were then saved and exported to CloudCompare software for 3D image analysis. Following the study conducted by Teh and Hamzah (2019), the 3D models were first converted into grey scales to reduce the model multidimensional domain to lower dimensions comprising only one or two component axes. For classification of the model, the threshold range values for adhesive failures and broken aggregates were determined by limiting the number of segments between 0 and 255. Accordingly, lower band values represents binder areas, while higher intensities shows the stripped and broken aggregates. The number of pixel point clouds attributed to broken aggregates, adhesive and cohesive failures was analysed and determined in CloudCompare. The calculated pixels by the software were then used to measure the portion of adhesion and cohesion failures as well as broken aggregates. For ease of

differentiating the composition of each specimen, white colour indicates the composition of broken aggregates, while red and black colours visualize the adhesive and cohesive failures, respectively. Figures 5a and b show the original 3-D model and classified model, respectively as obtained from CloudCompare software.

3. Results and Discussion

3.1 Compaction Energy and Workability Indices

Figures 6a and b show the CEI and WI of unconditioned asphalt mixtures produced with normal and cubical aggregates, respectively. The results presented in Figure 6a indicate that the CEI of HNU is considerably higher than WNU, while the difference between the corresponding values drops for HCU and WCU. The discrepancy between CEIs' of HNU and WNU implies that HMA requires extra energy for mixture compaction to achieve the desired density during road construction.

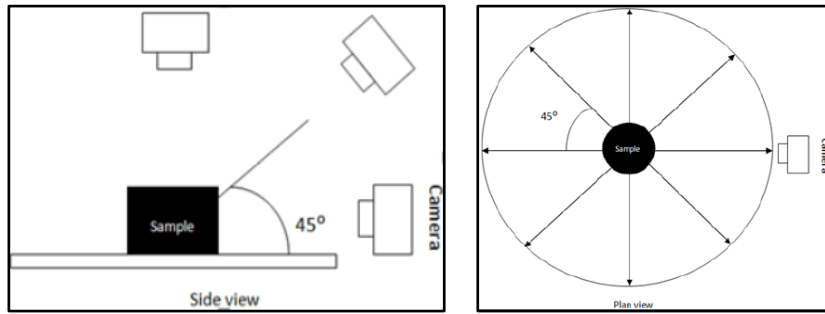


Figure 4. Schematic of the image capturing of the specimens' fractured surface

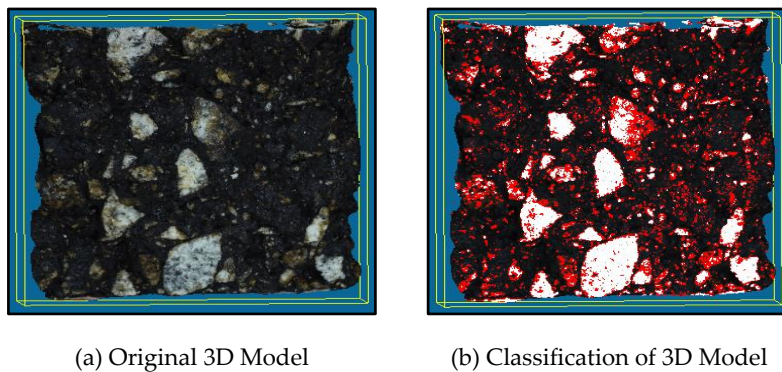


Figure 5. Image analysis using cloud compare

This finding is in agreement with the study conducted by Omranian et al. (2018b), where such behaviours were attributed to the beneficial impacts of warm mix additives on the CEI. In addition, the mixtures incorporating cubical aggregates exhibit lower CEI than mixtures produced with normal aggregates. This finding can be correlated to the shape of cubical aggregates that possesses higher homogeneity degree with visible edges and corners faces for dense packing and lower air voids. The difference between the CEI of HCU and WCU is noticeably lower when compared to similar HNU and WNU values. It indicates that cubical aggregates significantly reduce

the CEI, hence, the impacts of mixture type on the corresponding value can be ignored. The result in Figure 6b indicates that the WI of HNU and HCU is lower compared to the corresponding values of WNU and WCU, respectively. Despite the CEI, the difference between WI is more obvious for mixtures produced using cubical aggregates. It indicates that mixtures containing warm mix additive are more workable. In addition, mixtures prepared with cubical aggregates exhibits higher WI compared to mixtures produced using normal aggregates, which indicates improved workability of mixtures with cubical aggregates. The difference between the WI of mixtures with normal aggregates

is extremely lower compared to the corresponding values of mixtures produced with cubical aggregates. It

implies that mixture type has a more significant impact on mixtures containing cubical shape aggregates.

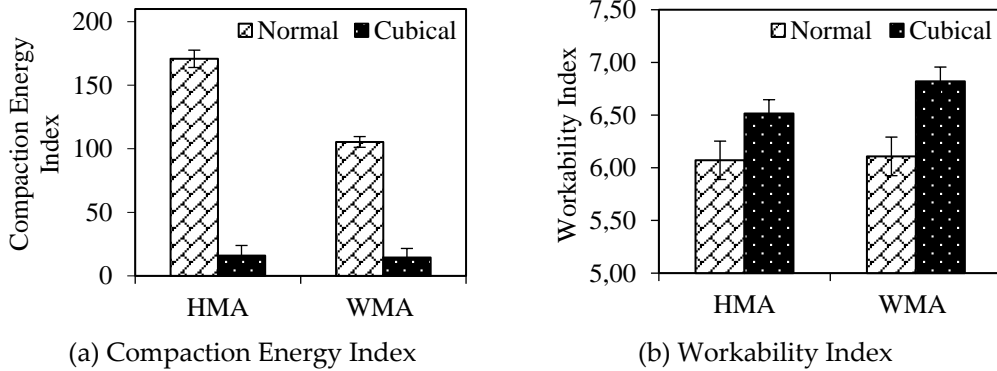


Figure 6. Results of mixture compactability indices

3.2 Shear Strength

Figures 7a and b illustrate the results of mixtures' shear strength and their ratio obtained from Leutner shear strength test, respectively. Figure 7a shows the higher shear strength of WMA over HMA for both conditioned and unconditioned samples. This outcome proves the effectiveness of the added warm mix additive that enhances the mixtures shear strength. It can also be correlated to the mixtures internal friction increment due to the warm mix additive. However, similar to the study conducted by Bennert *et al.* (2010), who detected increase in shear rate of binders incorporating Rediset as a warm mix additive that led to changes in internal friction of mixtures particles, further analysis should be carried out to substantiate such inferences. Moreover, the incorporation of cubical aggregates promotes shear strength for both HMA

and WMA based on the increase in corresponding values at about $10 \pm 1\%$ for all samples. This may be attributed to the cubical aggregates that contribute to enhanced shear stress resistance over the flaky and elongated shapes of normal aggregates. This implicates the beneficial impacts of cubical aggregates on the shear strength of mixtures. Figure 7a also shows that conditioning of mixtures (aging and moisturizing) decreases the shear strength, whereby the corresponding values reduce by almost $8 \pm 1\%$ for all samples. It can be concluded that aggregate shape exhibits a more significant effect on shear strength compared to aging conditions based on the higher percentage of aggregate effects on shear strength. Figure 7b compares the shear strength ratio of samples which also ranks the aging resistance of the specimens. The highest ratio is related to WCs followed by HCs, HNs and WNs. It implies that

although the differences are small (the maximum discrepancy is 1.22% which can be neglected), aging is less severe for mixtures produced using cubical aggregates. This can be attributed to the lower air voids in mixtures containing cubical aggregates which reduce the destructive impacts of moisture and aging on the samples. Figure 7b also shows that the least aging effects are related to WMA with normal aggregates, attributed to the minor undesirable effects of the added warm

mix additive (due to low additive dosage) that reduces the mixture resistance against moisture damage and aging. However, such inferences require further analysis since WMA with cubical aggregates exhibits lower susceptibility to moisture and aging damage compared to HMA produced with cubical aggregates, which can be correlated to the interaction of cubical aggregates with warm mix additive that enhances the mixtures aging resistance.

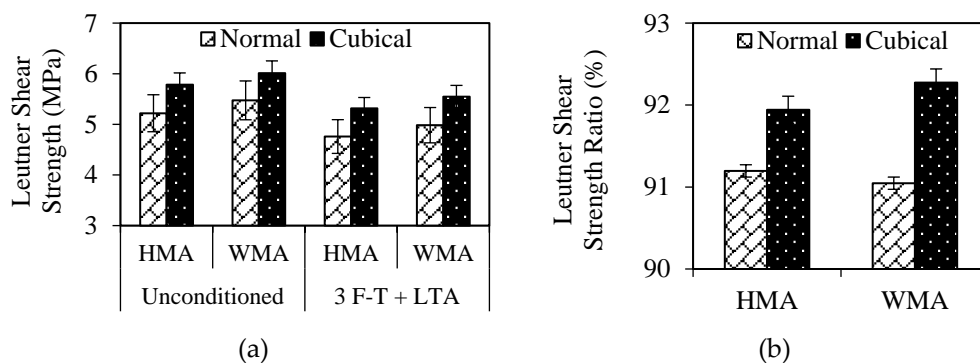


Figure 7. Results of Leutner shear strength and ratio

3.3 Tensile Strength

The fracture behaviour of samples in terms of tensile strength and their ratio is presented in Figures 8a and b, respectively. From Figure 8a, WCU and HNC respectively exhibits the maximum and minimum tensile strength. This trend is similar to a study conducted by Yang *et al.* (2017) who reported warm mix additive (Evotherm®) positive impacts on the tensile strength, moisture damage resistance, and fatigue performance of crumb rubber modified mixture. The results also show that there is a minor

favourable impact of cubical aggregates on the shear strength, while aging noticeably deteriorates the mixture fracture resistance, where the tensile strength is reduced by approximately $7.5 \pm 0.5\%$ for all mixtures after conditioning. Figure 8b shows the tensile strength ratio which associates with the difference between the aging resistance of mixtures. The highest tensile strength ratio is related to WCs followed by WNs, HCs, and HNs. Although the differences in results are not considerable (the maximum discrepancy is 0.864%), aging is less severe for WMA. It indicates the positive impacts of warm mix additive

on the mixtures resistance against the damages caused by moisture and aging conditioning. This finding is further explored using imaging technique. Figure 8b shows that the highest aging impacts are related to HMA with normal aggregates as reflected in the lowest tensile strength ratio. This certifies both cubical aggregate and warm mix additive constructive impacts to reduce

the moisture and aging resistance of mixtures. The effects of cubical aggregates on the tensile strength ratio can be directly correlated to such mixtures lower air voids. This finding is in agreement with the study conducted by Isacsson and Zeng (1998), where higher air voids resulted in higher aging rate and consequently reduced the mixtures fracture resistance.

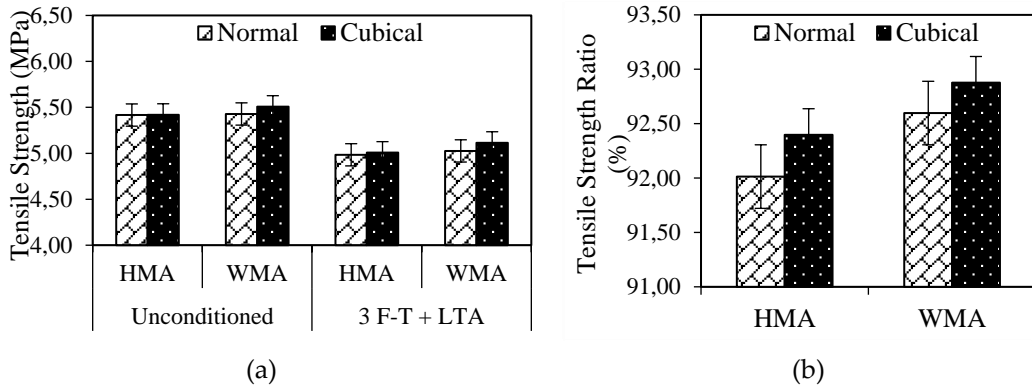


Figure 8. Results of tensile strength and ratio

3.4 Image Analysis

Image analysis was conducted on the fractured surfaces of samples to quantify the percentages of adhesive and cohesive failures as well as broken aggregates. Out of the three, this paper only presents the adhesive failure and broken aggregates results as shown in Figures 9 to 10. Cohesive failure can be easily calculated by deducting adhesive failure and broken aggregates summation from 100%. The results of image analysis representing adhesive failure of specimens tested by Leutner shear and SCB tests are illustrated in Figures 9a and b, respectively. These figures clearly show that conditioning of samples increases the adhesive failure

which can be associated with the destructive impacts of moisture damage and aging that weaken the adhesive bond between binder and aggregates, and consequently deteriorate the mixtures performance. The results also indicate that the incorporation of cubical aggregates reduces the adhesive failure of all mixtures. For instance, adhesive failure of HNUs tested using Leutner shear and SCB tests are 17,72% and 10.09%, respectively, while the corresponding values for HCUs decrease to 13,28% and 8,67%, respectively. This finding can be correlated to the variations in mixtures air voids and aggregate interlock based on the changes in aggregates geometrical shape. However, using either

conventional methods or advanced technologies such as utilization of X-ray computed tomography to scan and determine the mixtures' internal structures is recommended to prove such inferences. In addition, WMAs exhibit better performance in terms of adhesive failure compared to HMAs. This finding confirms the beneficial impacts of the added warm mix additive on mixtures to reduce the adverse impacts of moisture damage and aging. Although the trend of variation in mixtures adhesive failure remains unchanged for both tests, the samples subjected to shear test exhibit higher

adhesive failure compared to those studied through tensile strength test. For instance, adhesive failures of WCU and WCC tested using Leutner shear test are 11.98% and 13.22%, respectively, while the corresponding values are 10.19% and 8.18%, respectively, for SCB tested samples. It shows that adhesion plays a crucial role in mixture shear strength. Hence, incorporation of the warm mix additive as an antistripping agent is recommended for pavement that requires higher shear strength and locations that experience heavy rainfall to reduce pavement distresses due to moisture damage.

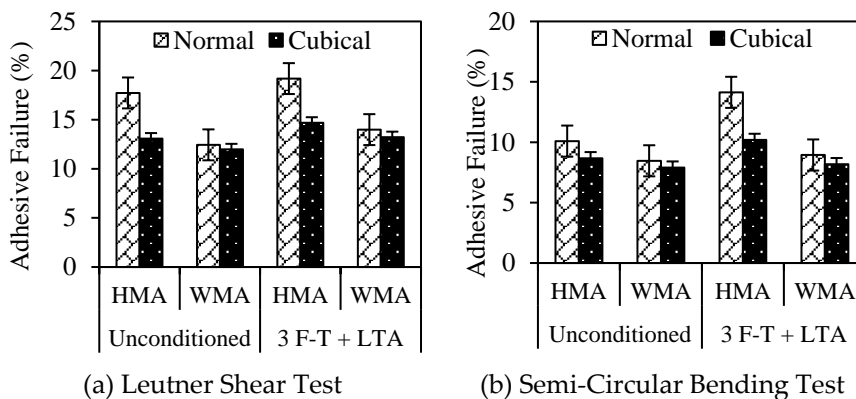


Figure 9. Adhesive failure of samples subjected to different performance tests

The percentages of the specimens' broken aggregates tested by Leutner shear and SCB tests are depicted in Figures 10a and b, respectively. The results show that the proportion of broken aggregates increases after conditioning which can be attributed to the destructive impacts of moisture and aging damages on the aggregates. In addition, lower percentages of broken aggregates are observed for samples produced using cubical shaped

aggregates. Although the differences between broken aggregates for WNC and WCC when tested using Leutner shear as well as HNU and HCU when tested by SCB are very small, the lower percentage of broken cubical aggregates can be correlated to their better interlock and lower proportion of flaky and elongated aggregates compared to normal aggregates. These figures also indicate that the proportion of broken aggregates varies by mixture type,

conditioning and test variation. For instance, in the case of samples subjected to the Leutner shear test, HCU exhibits slightly lower broken aggregates compared to WCU, while the corresponding value is higher for HCU over WCU when the SCB test was performed. An opposite trend can be observed in the case of HCC and WCC. Although no specific trend can be detected in the percentage of broken aggregates, the differences between proportions of broken aggregates for HMAs and WMAs at similar conditions are very low when Leutner shear test was conducted, and which can even be neglected. It can therefore be inferred that the use of warm mix additive may not exhibit substantial impacts on the

shear strength when the mixtures incorporate cubical aggregate. Such inference can be interpreted as the dominant impacts of aggregates on mixtures over warm mix additive. Moreover, the results indicate that the mixture has higher broken aggregates when tested by Leutner shear test compared to SCB test. For instance, the percentages of broken aggregates for HNU and WNU are 8.30% and 10.77%, respectively, when subjected to shear strength test, while the corresponding values are 7.56% and 8.08%, respectively, on SCB tested samples. It indicates that aggregates with higher cohesive strength should be incorporated when the mixtures are exposed to extreme shear distresses.

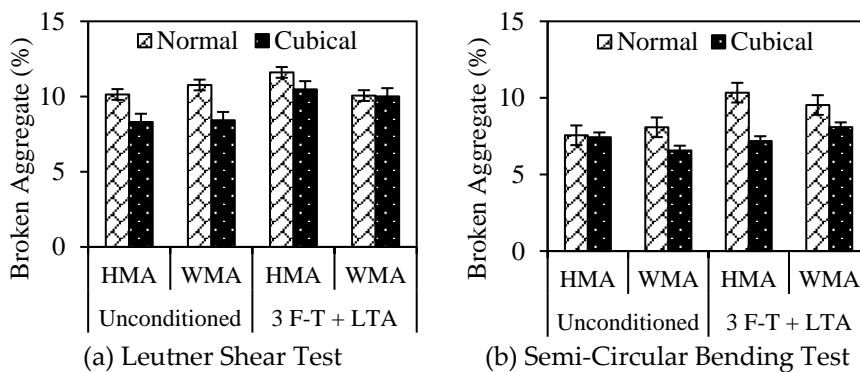


Figure 10. Broken aggregates of samples tested using different performance tests

4. Conclusions

Moisture damage susceptibility has always been a concern in asphalt mixes as the intrusion of water in asphalt pavement would eventually lead to pavement distresses such as stripping

and ravelling. The effectiveness and impacts of the added warm mix additive as an anti-stripping agent and a warm mix asphalt compaction additive on the mixtures moisture damage were investigated in this study. The effects of aggregate shape on the mixtures

engineering properties were also studied in terms of tensile and shear strengths, aggregate degradation after applied loadings and moisture susceptibility. The findings conclusions are as follows:

1. The WMA was more workable and easier to be compacted to the desired density as compared to HMA even at a lower compaction temperature, as reflected in the lower CEI and higher WI.
2. The WMA samples subjected to that exposed to simultaneous long-term aging and moisture damage exhibited better behaviour in terms of tensile and shear strength ratios compared to HMA. This proved the effectiveness of incorporating warm mix additive to reduce moisture damage in asphalt mixtures.
3. Mixtures incorporating cubical aggregates exhibited higher tensile and shear strengths than those produced with normal aggregates which implied cubical aggregates superior fracture resistance when subjected to applied loads.
4. The adhesive failure of WMA incorporating cubical aggregates was lower than HMA. This implicated that the utilization of warm mix additive and cubical aggregates enhanced the mixtures moisture damage resistance.
5. The percentage of broken aggregates was found to be independent of moisture conditioning and mixture type since no specific trends were observed. The higher percentage of broken aggregates was found in mixtures incorporating normal aggregates compared to those containing cubical aggregates due to

higher proportion of flaky and elongated aggregates.

Acknowledgements

The authors would like to acknowledge the Malaysian Ministry of Higher Education for funding this research through the Fundamental Research Grant Scheme FRGS/2/2013/TK07/USM/01/1 which enables this paper to be written.

References

- AASHTO (2014). AASHTO T 164, Standard Method of Test for Quantitative Extraction of Asphalt Binder from Hot Mix Asphalt (HMA), American Association of State and Highway Transportation Officials, Washington D.C.
- AASHTO (2016). AASHTO TP 124, Standard Method of Test for Determining the Fracture Potential of Asphalt Mixtures using Semi-Circular Bend Geometry (SCB) at Intermediate Temperature, American Association of State and Highway Transportation Officials, Washington D. C.
- Arefin, M. S., Quasem, T., Nazzal, M., Abbas, A. R., and AbuHassan, Y. (2018). Effect of Short-term and Long-term Ageing on Dynamic Modulus of Foamed Warm Mix Asphalt. *International Journal of Pavement Engineering*, 1-13.
- ASTM (2006). ASTM D4867, Standard Test Method for Effect of Moisture on Asphalt Concrete Paving Mixtures, ASTM International, West Conshohocken, PA, USA.
- Bairgi, B. K., Tarefder, R. A., and Ahmed, M. U. (2018). Long-term Rutting and Stripping Characteristics of Foamed Warm-Mix Asphalt (WMA) through Laboratory and Field Investigation. *Construction and Building Materials*, 170, 790-800.

- Barraj, F., Khatib, J., Castro, A., and Elkordi, A. (2022). Effect of Chemical Warm Mix Additive on the Properties and Mechanical Performance of Recycled Asphalt Mixtures. *Buildings*, 12(7), 874.
- Bell, C.A., AbWahab, Y., Cristi, M.E. and Sosnovske, D. (1994). Selection of Laboratory Aging Procedures for Asphalt-Aggregate Mixtures, Strategic Highway Research Program, Report No. SHRP-A-383, Washington, D.C.
- Bennert, T., Reinke, G., Mogawer, W., and Mooney, K. (2010). Assessment of workability and compactability of warm-mix asphalt. *Transportation Research Record: Journal of the Transportation Research Board*, (2180), 36-47.
- Cabrera, J. G. (1991). Assessment of the Workability of Bituminous Mixtures. *Highways and Transportation*, 38(11).
- Copeland, A., Youtcheff, J. and Shenoy, A. (2007). Moisture Sensitivity of Modified Asphalt Binders: Factors Influencing Bond Strength, *Transportation Research Record: Journal of the Transportation Research Board*, Vol. 1998, No. 1, pp. 18-28.
- Dessouky, S., Pothuganti, A., Walubita, L. F. and Rand, D. (2012). Laboratory Evaluation of the Workability and Compactability of Asphaltic Materials Prior to Road Construction. *Journal of Materials in Civil Engineering*, 25(6), 810-818.
- Hamzah, M. O., Omranian, S. R., and Golchin, B. (2015). A Review on the Effects of Aging on Properties of Asphalt Binders and Mixtures. *Caspian Journal of Applied Sciences Research*, 4(6).
- Hamzah, M.O., Lo, S.S., You, Z., Hasan, M.M. and Abdullah, N.H. (2014). Effects of Geometrically Cubical Shaped Aggregate on the Engineering Properties of Porous Asphalt. *Sains Malaysiana*, Vol. 43, No. 2, pp. 303-312.
- Hamzah, M.O., Puzi, M.A.A. and Azizli, K.A.M. (2010). Properties of Geometrically Cubical Aggregates and Its Mixture Design. *IJRRAS*, Vol. 3, No. 3, pp. 249-256.
- Hicks, R.G. (1991). Moisture Damage in Asphalt Concrete, NCHRP Synthesis 175, Transportation Research Board. National Research Council, Washington, D.C.
- Isacsson, U., and Zeng, H. (1998). Cracking of Asphalt at Low Temperature as related to Bitumen Rheology. *Journal of Materials Science*, 33(8), 2165-2170.
- Izadi, A., Motamedi, M., Alimi, R., and Nafar, M. (2018). Effect of Aging Conditions on the Fatigue Behavior of Hot and Warm Mix Asphalt. *Construction and Building Materials*, 188, 119-129.
- JKR (2008). Standard Specification for Road Works, Section 4: Flexible Pavement, Jabatan Kerja Raya, Kuala Lumpur.
- Kuan, K.P. (2017). Evaluation of Moisture Sensitivity of Asphalt Mixtures Incorporating Different Anti-Stripping Additives Subjected to Various Conditioning Methods. Undergraduate Thesis, School of Civil Engineering, Universiti Sains Malaysia, Nibong Tebal, Penang.
- Mahmoud, A.F.F., and Bahia, H., (2004). Using the Gyratory Compactor to Measure Mechanical Stability of Asphalt Mixtures. *WHRP 05-02*. University of Wisconsin, Madison.
- Menapace, I., Masad, E., Bhasin, A., and Little, D. (2015). Microstructural Properties of Warm Mix Asphalt before and after Laboratory-simulated Long-term Ageing. *Road Materials and Pavement Design*, 16(sup1), 2-20.
- Omranian, S. R., Hamzah, M. O., and Hasan, M. R. M. (2017). Introducing New Indicators to Evaluate Fracture Properties of Asphalt Mixtures Using Semicircular Bending Test. *Iranian Journal of Science and Technology, Transactions of Civil Engineering*, 1-9.
- Omranian, S. R., Hamzah, M. O., Gungat, L., and Teh, S. Y. (2018b). Evaluation of asphalt mixture behavior incorporating warm mix additives and reclaimed

- asphalt pavement. *Journal of Traffic and Transportation Engineering (English Edition)*.
- Omranian, S. R., Hamzah, M. O., Valentin, J., and Hasan, M. R. M. (2018a). Determination of optimal mix from the standpoint of short term aging based on asphalt mixture fracture properties using response surface method. *Construction and Building Materials*, 179, 35-48.
- Rohith, N. and Ranjitha, J. (2013). A Study on Marshall Stability Properties of Warm Mix Asphalt using ZycoTherm a Chemical Additive, *International Journal of Engineering Research & Technology (IJERT)*, ISSN, pp. 2278-0181.
- Sharanappanavar, M.S. (2013). Study on Behavior of Warm Mix Asphalt Using ZycoTherm. *International Journal of Science and Research (IJSR)*, ISSN 2319-7064, pp. 2319-7064.
- Sudarsanan, N., Karpurapu, R., and Amrithalingam, V. (2018). An Investigation on the Interface Bond Strength of Geosynthetic-reinforced Asphalt Concrete Using Leutner Shear Test. *Construction and Building Materials*, 186, 423-437.
- Teh, S. Y., and Hamzah, M. O. (2019). Asphalt Mixture Workability and Effects of Long-term Conditioning Methods on Moisture Damage Susceptibility and Performance of Warm Mix Asphalt. *Construction and Building Materials*, 207, 316-328.
- Valentová, T., Altman, J., and Valentin, J. (2016). Impact of Asphalt Ageing on the Activity of Adhesion Promoters and the Moisture Susceptibility [online]. *Transportation Research Procedia.*, 0(14), pp. 768-777. ISSN 2352-1465. Available from:
<http://www.sciencedirect.com/science/article/pii/S2352146516300667>
- Wen, H., Wu, S., Mohammad, L. N., Zhang, W., Shen, S., and Faheem, A. (2016). Long-term Field Rutting and Moisture Susceptibility Performance of Warm-Mix Asphalt Pavement. *Transportation Research Record: Journal of the Transportation Research Board*, (2575), 103-112.
- Yang, X., You, Z., Hasan, M. R. M., Diab, A., Shao, H., Chen, S., and Ge, D. (2017). Environmental and Mechanical Performance of Crumb Rubber Modified Warm Mix Asphalt Using Evotherm. *Journal of Cleaner Production*, 159, 346-358.